ESTONIAN UNIVERSITY OF LIFE SCIENCES
Institute of technology

Toivo Viidalepp

FABRICATION OF A PROTOTYPE DEVICE FOR PHOTOCURRENT GENERATION USING HfO_2-CNT NANOHYBRIDS AS THE ACTIVE LAYER

PROTOTÜÜPSEADE FOTOGALVAANILISE EFEKTIGA VOOLU TEKITAMISEKS KASUTADES AKTIIVSE KIHINA HfO_2-SÜSINIK-NANOTORUDE HÜBRIIDE

Master's thesis
Energy Application Engineering

Supervisor: Protima Rauwel, *PhD*
Co-supervisor: Alo Allik, *PhD*
Co-supervisor: prof. Erwan Rauwel, *PhD, DSc*

Tartu 2020

www.emu.ee

Eesti Maaülikool

Estonian University of Life Sciences

Eesti Maaülikool Kreutzwaldi 1, Tartu 51006		Magistritöö lühikokkuvõte	
Autor: Toivo Viidalepp		Õppekava: Energiakasutus	
Pealkiri: Prototüüpseade fotogalvaanilise efektiga voolu tekitamiseks kasutades aktiivse kihina HfO_2-süsinik-nanotorude hübriide			
Lehekülgi: 57	Jooniseid: 24	Tabeleid: 6	Lisasid: 1
Osakond / Õppetool: Energiakasutuse õppetool ETIS-e teadusvaldkond ja CERC S-i kood: 4. Loodusteadused ja tehnika 4.17. Energeetikaalased uuringud T140 Energeetika Juhendaja(d): Protima Rauwel, *PhD*; Alo Allik, *PhD*; Prof. Erwan Rauwel, *DSc*, *PhD* Kaitsmiskoht ja -aasta: Tartu 2020			
Selle magistritöö eesmärk oli luua prototüüpseade nanohübriidmaterjalide, nagu HfO_2-süsinik-nanotorud (CNT), poolt tekitatud fotovoolu mõõtmiseks. Seadme ülesandeks oli valgustada nanohübriidmaterjali proovi ultraviolett- ja nähtava valgusega ning tavapärase multimeetri abil mõõta mõne nanoampri suurust fotovoolu. Praegu teada olevalt ei ole sellise uurimistegevuse jaoks kaasaskantavaid seadmeid koos vajalike komponentide ja spetsifikatsioonidega saadaval. Ühes eelnevas uuringus tuvastati, et 1 mg nanohübriid-materjali võib tugeva valgustatuse korral tekitada fotovoolu umbes 150 nA, mis on enamiku multimeetrite lahutusvõime piiril. Uuringu eesmärk oli mõõta nanoamprite suurusjärgus voolu kahe erineva tehnilise tasemega EMÜ-s saadaoleva multimeetri abil. Selle saavutamiseks koostati operatsioonivõimendiga vooluahel, mis võimendab šunttakisti pingelangu, mida saab mõõta multimeetri mV pingevahemikus ja mis vastab võimendi sisendi nA väärtusele. Seadme arendusfaasis valmisid neli prototüüpi ja lõplikul prototüübil on valgustusseade, mille väljundvõimsus on 339 W / m^2 ning voolu eraldus-võime 0,01 nA. Prototüübi väljatöötamise lahutamatu osa oli häirete vähendamine, mille käigus vähendati neid 50 nA pealt 1,7 nA peale.			
Märksõnad: Fotovool, Süsiniknanotorud, nanoamper, HfO_2, Operatsioonivõimendi			

www.emu.ee
Eesti Maaülikool
Estonian University of Life Sciences

Estonian University of Life Sciences Kreutzwaldi 1, Tartu 51006		Abstract of Master's Thesis	
Author: Toivo Viidalepp		Curriculum: Energy Application Engineering	
Title: Fabrication of a Prototype Device for Photocurrent Generation Using HfO_2-CNT Nanohybrids as the Active Layer			
Pages: 57	Figures: 24	Tables: 6	Appendixes: 1
Department / Chair: Chair of Energy Application Engineering Field of research and (CERC S) code: 4. Natural Sciences and Engineering 4.17. Energetic Research T140 Energy research Supervisors: Protima Rauwel, *PhD*; Alo Allik, *PhD*; Prof. Erwan Rauwel, *DSc*, *PhD* Place and date: Tartu, 2020			
The goal of this Master's thesis was to create a prototype setup in order to measure the photocurrent generated by hybrid nanocomposites like HfO_2-carbon nanotube based (CNT). The specifications of the setup were to illuminate a sample with UV and visible light and to be able to measure photocurrent of a few nano-ampere using a conventional multimeter. No portable device for such research activity with the required components and specifications is available presently. It was demonstrated in a previous study, that 1 mg of the nanohybrid can, under strong illumination, produce a photocurrent of about 150 nA, which is on the resolution limit of most multimeters. The study aimed at obtaining current values with high accuracy with two different multimeters available at EMÜ. This was brought about by building a circuit with an operational amplifier that amplifies the voltage drop on a shunt resistor. The resulting voltage is measurable in mV range and corresponds to nA scale of the amplifier input. Four prototypes were developed, and the final prototype has a lighting unit with 339 W/m^2 power output and current measurement resolution of 0,01 nA. An integral part of the prototype development was the mitigation of interferences, which were brought down from 50 nA to 1,7 nA.			
Keywords: Photocurrent, Carbon nanotubes, nanoampere, HfO_2, Operational amplifier			

TABLE OF CONTENTS

ACRONYMS AND ABBREVIATIONS

c	–	Speed of light m/s
CNT	–	Carbon nanotubes
DIP8	–	Transistor dual in line packaging form with 8 pins
DMM	–	Digital multimeter
E	–	Photon energy eV
EM	–	Electromagnetic
EMU	–	Estonian University of Life Sciences (Eesti Maaülikool)
eV	–	Electronvolt
fA	–	Femtoampere
h	–	Planck's constant $4{,}135667696 \cdot 10^{-15}$ eV·s
HfO_2	–	Hafnium dioxide
HfO_2-CNT	–	Hafnium dioxide - carbon nanotube nanohybrid
IMEP-LaHC	–	Institute of Microelectronics, Electromagnetism, Photonics and Hyperfrequencies
ITO	–	Indium tin oxide
I-V Curve	–	Current - voltage curve
JFET	–	Junction Field Effect Transistor
λ	–	Wavelength, nm
LED	–	Light emitting diode
MINATEC	–	Micro- and Nanotechnology Research Centre in Grenoble Alpes University, France
MWCNT	–	Multi-walled carbon nanotubes
nA	–	Nanoampere
PV	–	Photovoltaic
STEM	–	Scanning transmission electron microscope
SWCNT	–	Single-walled carbon nanotubes
TEM	–	Transmission electron microscopes
TO-220	–	Transistor packaging form with 3 pins
TTÜ	–	Tallinn University of Technology (Tallinna Tehnikaülikool)
UV	–	Ultraviolet

1. INTRODUCTION

Nanohybrids are composite materials involving two different classes of nanomaterials, i.e. organic and inorganic material brought together by hybridizing. This process involves bonding of both classes of materials at an atomic level, which occurs at the interface of the two nanomaterials. In general, nanomaterials possess novel properties, compared to their bulk counterparts. For example, HfO_2 (inorganic) in general is not a photoluminescent material but when reduced to nanoparticles with sizes as small as 2-3 nm, they emit light in the visible part of the solar spectrum. In addition, nanohybrids possess properties consisting of each individual nanomaterial and novel properties created as a result of hybridizing. When HfO_2 nanoparticles are combined with carbon nanotubes (CNT), they are able to generate a current under photoexcitation. This photocurrent generation is absent in each of the individual materials, but their hybridization enables photocurrent generation. In previous works, this nanohybrid's ability to generate photocurrent under ultraviolet (UV) and visible light excitation was demonstrated [1]. This means that these nanocomposites have potential applications in solar energy harvesting and require further investigation.

CNT are nanomaterials that can be described by rolling sheets of graphene. CNT can have different properties depending on the way they were synthesized. In the current work, the photocurrent is generated by the combination of HfO_2 nanoparticles and CNT (HfO_2-CNT nanohybrid). This is a nanocomposite that needs to be characterized optoelectronically. It has already been a subject of interest for two other master's thesis topics in TTÜ: by Martin Salumaa in 2015 [2] and Andres Aasna in 2016 [3]. Nevertheless, measuring the photocurrent of these nanocomposites has always been tedious and requiring high-level instruments that are available at MINATEC, Grenoble, France. This is mainly because the currents emitted are in the nano- or microampere ranges due to the low quantities of materials measured, usually in milligram. Such nano-ampere currents are not detectable with conventional multimeters that are limited to microampere range and higher. The multimeters have a high voltage burden, which decreases precision when measuring at the lower end of a measurement range [4], [5]. Additionally, all measurements of currents in that range are susceptible to electromagnetic noise, which can be emitted by any power source or wires in the vicinity with currents higher than the one measured. Specific equipment exists for such precise measurements, but these instruments are expensive and are not easily accessible.

The purpose of this research project was to develop a setup that can measure such low currents as a routine with less specialized equipment. This will allow measuring the photocurrents generated by exciting nanohybrids with UV and visible light on site at EMÜ. The goal was to build a prototype measurement device that would enable scientists to routinely study these nanohybrids and further advance in their investigations. The equipment should have sufficient accuracy to support research activities for the future construction of prototype solar cells.

The following tasks needed to be completed:

- review the literature regarding photoluminescent nanohybrids to understand the requirements for the device;
- review the literature regarding the measurement of nanoscale or smaller currents and any available devices;
- select the most suitable substrates for easy manipulation and characterization of nanohybrid samples;
- build a prototype device with lighting and nanocurrent measurement capability;
- calibrate the device against a known high precision measurement device;
- validate the lighting density of the light source;
- reduce the noise produced by surrounding equipment.

This work was carried out under the Centre of Excellence project EQUiTANT (TK134): "Emerging orders in quantum and nanomaterials", exploring new nanomaterials and their potential applications [6].

Next, literature overview section introduces nanohybrids and reviews previously used measurement methods. In addition, possible substrates and usable measurement methods are discussed. In the materials and methods section, an overview of the planned device construction and the measurement procedure is given. The results section provides the process of building the device along with a critique on the same.

To measure the generated photocurrent, two different types of electrodes were tested: comb electrodes on an etched circuit board and indium tin oxide (ITO) coated glass electrodes sandwiched together to simulate a solar cell. For light excitation, LED lighting with a

wavelength of 372 nm and 400-700 nm was tested. To measure the current, a measurement pre-amplifier circuit with an operational amplifier was created and all electrical circuits were carefully shielded and grounded.

I would like to thank my supervisors Dr. Protima Rauwel, Dr. Alo Allik and Prof. Erwan Rauwel for their knowledge, guidance and support while writing this thesis. I would also like to acknowledge the Centre of Excellence project EQUiTANT (TK134) “Emerging orders in quantum and nanomaterials”. I am grateful to Dr. Frédérique Ducroquet for reviewing this manuscript and willing to welcome me to her laboratory, the staff at the University of Life Sciences in Tartu for their help and support, Archimedes Foundation's Kristjan Jaak short study visit programme and last but not least, I would like to thank my family for all the support and encouragement I received from them.

2. STATE OF THE ART

2.1. Introduction to nanomaterials

A material is considered a nanomaterial if at least one dimension of it is measured from 1 to 100 nm (10^{-9} m). If one dimension is in the nanoscale it's a nanoplate. If two of the dimensions are in nanometres, then it is a nanofibre and with all dimensions in nanoscale, it is called a nanoparticle [7], [8], [9]. Figure 1 shows a size comparison of some known objects. For example, in 2020 the modern processors in personal computers and smartphones are manufactured with 7 nm transistors and the SARS-CoV-2 virus has an average size of 100 nm.

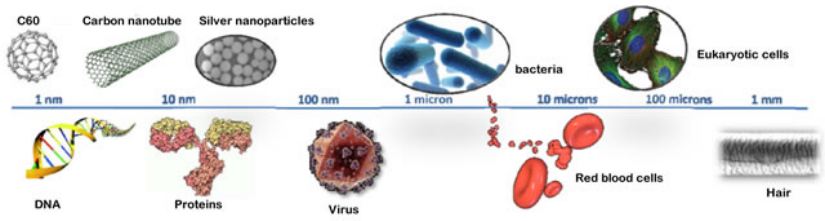

Figure 1. Size of some objects in nano- and microscale [10].

The dimension is a simple way to identify the material, but the size reduction effect to the nanoscale is the main focus of nanoscience. Nanohybrids, as previously explained, can display new properties arising from the combination of two different nanomaterials, where bonding at the atomic level has occurred.

The manufacturing process of nanohybrids is different from that of common alloys, but similar to composite materials. A composite material exhibits the properties of all substances it contains, and additional properties appear through a synergistic effect of their combination. However, in nanomaterials, the processing method can also affect nanoparticle's properties through their size reduction, defects present in the nanostructure or surface functionalization. [10]

Nanoparticles are not visible under light microscope as the diffraction barrier limits the observations to 200 nm [11]. They are therefore studied with scanning electron microscopy (SEM), transmission electron microscopes (TEM) and scanning transmission electron microscope (STEM) for atomic column resolution.

2.2. Synthesis of nanomaterials

Nanomaterials can be either of non-intentional (possibly natural) or intentional (synthesized) origin. Non-intentionally made nanomaterials are for example viruses [12], volcanic ash [13] and emissions from internal combustion engines [14], [15]. Intentionally made nanomaterials are those fabricated for some purpose. There are multiple ways to categorize the methods of synthesis. One classification offers a differentiation based on the direction of the process of the particle size change: top-down or bottom-up.

Compared to top-down method approaches, bottom-up approaches are more numerous. Figure 2 displays the different categories of bottom-up approaches that are divided into physical, chemical and biological methods. The HfO_2 nanoparticles used in this thesis as test samples were synthesized by a non-aqueous sol-gel process method, which is a chemical approach [16].

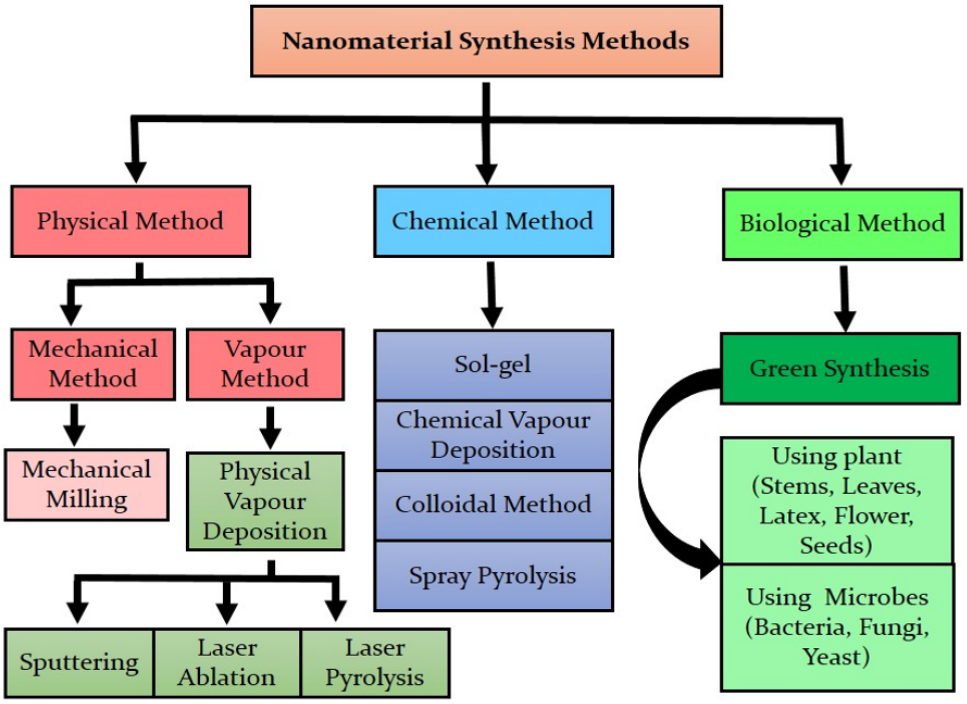

Figure 2. Methods of nanomaterial synthesis [17].

The physical methods involve only mechanical methods, which are among the few top-down methods. Mechanical milling consists of grinding bulk material in powder form into nano-sized particles. The process is relatively simple, well scalable and cost-effective. However,

the size distribution of the nanoparticles is quite broad, and their shape is non-uniform. The same process is used for creating fine powders, such as pigments or cement and for separating metals from ores [18], [19]. Another physical method is vapour deposition, a gas phase process where bulk material is evaporated by heating, using a laser or by means of ion sputtering [20]. The evaporation can take place in a liquid solution or in vacuum. The produced nanoparticles are collected by condensation or using a filter for example.

There are many chemical methods available for nanoparticle synthesis. These methods can be divided into gas phase and liquid phase processes [19]. One of the gas phase processes known as chemical vapor deposition generates particles with reactions of chemical precursors.

The important method in regard to the work done in this thesis is the sol-gel method. This is a wet chemical process that is mainly used for the synthesis of metal oxides nanoparticles and ceramic powders with high purity and homogeneity. During this process a solution containing metal nanoparticles forms a colloidal suspension (sol) and is converted into a wet solid-like substance (composition and density similar to a liquid, cohesiveness similar to a solid) similar to a viscous gel. Sol-gel processes are affected by many parameters: pH, solvent, temperature (both external and reaction-generated), time, catalyst and agitation. The main advantage is the versatility of the method that enables to process the “gels” into various forms (powders, fibres, ceramics and coatings) by drying the gel and processing it. [19], [21], [22]

The non-aqueous sol-gel process was developed to overcome some disadvantages of the aqueous sol-gel process, like problems with controlling the rapid hydrolysis of metal precursors, an extra calcination step to induce crystallization but that induces the agglomeration of the nanoparticles and overall complexity. The non-aqueous method allows the use of different precursors, for example inorganic metal salts, acetates and alkoxides. These slow down the hydrolysis and as a result allow better control over the reaction on a molecular level and therefore enable the synthesis of nanoparticles of uniform size, well-defined shape and high crystallinity. [23], [24]

Biological methods involve the use of biomolecules present in the plants or use bacteria, fungi or yeast as medium for the synthesis of nanoparticles. The common benefit of these

methods is the eco-friendliness. The most versatile method involves plant extracts because the utilization of micro-organisms requires more management during cultivation and more preparation before use. This makes the processes using micro-organisms more difficult to scale up and usually the size distribution of synthesized nanomaterials is broader than in the case of plant extracts utilization. The plant extract-based methods are based on the utilization of enzymes, amino-acids, vitamins or proteins that are present in plants and can be conducted at ambient temperature without the need of special equipment. A large number of plant extracts have been investigated and it is possible to obtain a synergistic effect because some properties of the plant, such as anti-inflammatory or antibacterial properties can be combined with the intrinsic properties of the produced nanoparticles [25]. [17], [24], [26]

2.3. Nanohybrids

CNT were first reported in 1952 [27], but it was not possible to perform investigations on these new nanomaterials with the technology of that time. CNT were fully characterized in 1991 [27] and research has been extensive since then. CNT are sheets of graphene, one atom thin, which are rolled into tubes. Based on the number of graphene layers or the number of times a single graphene sheet is rolled, they produce either single-walled carbon nanotubes (SWCNT) or multi-walled carbon nanotubes (MWCNT). Depending on their type and manufacturing method, SWCNT can be either semiconducting or conducting (metallic) and MWCNT are always metallic [28]. In this study, MWCNT were chosen for their conductivity that enables to extract and lead away the charges generated by HfO_2 nanoparticles to an external load.

CNT are often used as substrates to create nanohybrids by combining CNT with other nanomaterials. The nanoparticles can attach to defects present on CNT surface through Van der Waals interactions. The faults are places of defects on CNT where the outer wall is not intact and include breaks, kinks, bends, deformations, branches, atomic vacancies or interstitial atoms. Van der Waals interactions are very weak close-range electrostatic forces between atoms or molecules, which are not ionic or covalent and do not form chemical bonds [29], [30]. There are not many defects in as-synthesized CNT, so these defects have to be generated. The process of adding defects to the sidewalls of CNT is known as functionalization. In a previous master's thesis, Martin Salumaa (2015) [2] studied the

functionalization of MWCNT by ultrasonication (stirring the particles in the solution with ultrasound) and created nanohybrids with HfO_2. His goal was to study how the sonication time affects the MWCNT and test the resulting nanohybrid for photocurrent generation. The photocurrent generation was confirmed under a strong UV-light for a sample sonicated for 30-minutes [2]. The electronic properties of CNT and CNT-HfO_2 nanohybrids were further studied in an article published in 2016 [1]. Salumaa's findings were reproduced and taken further by Andres Aasna in his master's thesis (2016) [3], where he tested nanohybrids with HfO_2 and ZnO and confirmed photo-response with HfO_2-CNT nanocomposites only [3].

Hafnium (Hf) is chemically very close to zirconium (Zr). Hafnium's existence was presumed in 1869 by Mendeleev and confirmed in 1923 by Coster and Hevesy in Copenhagen. Hafnium was named after the city it was discovered in, which is *hafnia* in Latin. While zirconium is transparent to thermal neutrons and is used in metal components of nuclear reactors, hafnium also absorbs neutrons and is used in the control rods of a nuclear reactor. For that reason, hafnium has to be separated from zirconium before it can be used. Recent studies showed that HfO_2 is not considered toxic. [31], [32], [33]

Hafnium dioxide-based compounds are dielectrics and have been used since 2007 in integrated circuits as chemical components of the gate dielectrics in transistors to reduce gate leakage current [34]. HfO_2 in bulk form is optically inactive, but in nano-size exhibits photoluminescent properties [11-12] and is able to generate photocurrent [1], [36]. HfO_2 nanoparticles with a cubic structure and with sizes of about 2,6 nm were used in this study [16].

2.4. Sample substrates

Substrates are needed to transmit the charges from the nanocomposite to the load where the current is generated. In previous works, where photocurrent was measured, silicon, glass or copper substrates were used to measure the produced photocurrent. Martin Salumaa in 2015 [2] used silicon substrates with probes directly in contact with the CNT sample near an area that emitted photoluminescence under UV excitation on the test sample. Andres Aasna in 2016 and Rauwel et. al. in an article of 2016 used glass substrates with probes in contact with the CNT sample [1], [3]. Rauwel et. al. in an article of 2019 used copper electrodes

consisting of two conductive copper pads with a space between them, where the sample was deposited. The space between the electrodes was 1-2 millimetres, and the probes were positioned on the copper pads, away from the CNT measured [36].

In this thesis, comb electrodes etched out of a copper circuit board and indium tin oxide (ITO) covered glass sheets were used as substrates. The copper circuit board electrodes were chosen because they are easy to make in any suitable configuration and could later be ordered from a professional manufacturer, if necessary. ITO glass is a glass piece, usually 1,1 mm thick, that has a conductive 100 nm layer of ITO on [37]. Different configurations of thickness and conductivity are available. It was chosen because the response of such substrate is very similar to PV cell [38].

Comb electrodes are commonly used for biosensors and dielectric sensors, which makes them suitable for nanohybrids study as well [39], [40]. ITO-covered glass with or without printed comb-like electrodes is used by Ossila company for prototyping solar cells [41].

2.5. Illumination and measurement of the sample

In former studies, strong lighting has been used. A 10 mW He-Cd laser emanating at 325 nm was used to investigate the photoluminescence process of HfO_2 and its nanohybrids [16], [35]. In 2019, a 125 W Hg lamp emanating at 365 nm was used for testing photocurrent generation under UV light and maximum of 200 nA photocurrent was measured from about 1 mg of HfO_2 CNT nanohybrid. In the same study, photocurrent generation under visible light was also measured at wavelengths of 475 nm (blue) and 575 nm (yellow), which resulted in a 100 nA photocurrent [36]. The electrical measurements were performed on an Agilent 4156C Semiconductor Parameter Analyzer with a 0,01 fA (one femto-ampere equals 10^{-15} A) DC current resolution [42].

Figure 3 shows a Tauc plot with the relation of optical absorption strength ($(\alpha h\nu)^2$) to photon energy (E, eV). The photon energy can be converted into wavelength and this will show the wavelengths where the sample absorbs using the DeBroglie wavelength formula: [43], [44]

$$\lambda = \frac{h \cdot c}{E}, \quad (1)$$

where λ is the wavelength nm;

h – Planck's constant 4,135667696·10^{-15} eV·s;
c – speed of light 299792458 m/s;
E – photon energy eV.

For better readability in the following calculations, here is $h \cdot c$ calculated:

$$h \cdot c = 4{,}135667696 \cdot 10^{-15} \cdot 299792458 = 1239{,}84$$

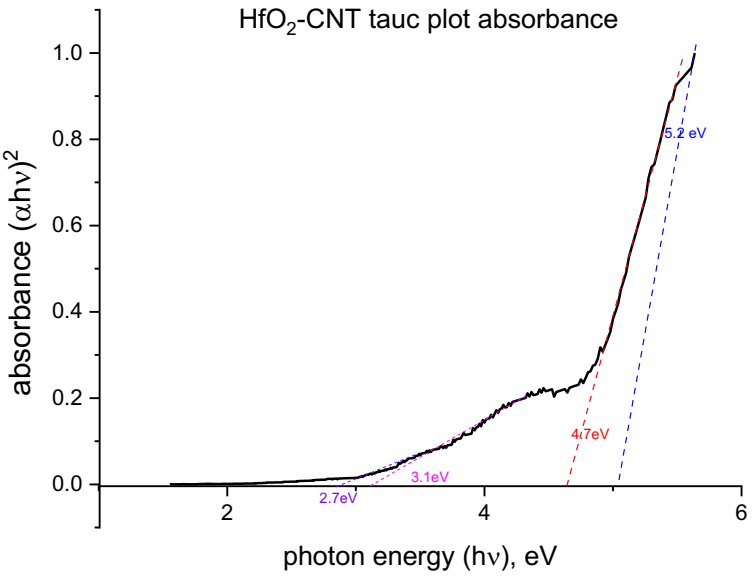

Figure 3. Tauc plot of CNT-HfO_2 used in this study. The sample absorbs at various wavelengths (λ_1 = 2,7 eV; λ_2 = 3,1 eV; λ_3 = 4,7 eV; λ_4 = 5,2 eV).

The calculated wavelengths of the plot:

$$\lambda_1 = \frac{1239{,}84}{2{,}7} = 459{,}20 \text{ nm}$$

$$\lambda_2 = \frac{1239{,}84}{3{,}1} = 399{,}95 \text{ nm}$$

$$\lambda_3 = \frac{1239{,}84}{4{,}7} = 263{,}80 \text{ nm}$$

$$\lambda_4 = \frac{1239{,}84}{5{,}2} = 238{,}43 \text{ nm}$$

The linear regression, where the tangent parallel to absorption cliff intersects with the X-axis, gives absorption wavelengths of the material. At these wavelengths, photocurrents will be produced. Since most applications require visible light excitation, similarly to

photovoltaics, near UV-blue and visible light LEDs were chosen based on the Tauc plot absorbance for this thesis.

Martin Salumaa in 2015 and Andres Aasna in 2016 used a halogen lamp and a UV lamp and Andres Aasna measured 1-3 nA photocurrent from one sample. The measurement was taken with a HP 4155A semiconductor parameter analyser with a resolution of 10 fA [45]. These HP analysers were later called Agilent [46].

Nanoampere current measurement is generally associated with measuring standby power of low-power electronic components or leaking current of capacitors and transistors. Microelectronics enthusiast David Johnson-Davies has made a nanoammeter based on an ATtiny84 microcontroller for measuring sleep current of microcontrollers, which could work for the task at hand. Its measurement ranges from 30 nA to 10 μA and according to the author, is not as accurate as a circuit based on an operational amplifier [47]. A PV cell prototype measuring device available from Ossila can generate IV-curves but that has a resolution of 10 nA in a 150 mA measurement range but does not provide light excitation to the sample [48].

For the measurement part of this project, it was found that a pre-amplifier circuit involving an operational amplifier was deemed necessary to measure nanoampere currents. This solution would enable enhancing measurement resolution to below 1 nA with sufficient accuracy. The circuit was purposefully built in accordance with the currents measured and with the device displaying the measurement. Similar methodologies are used for reading picoamperes in a biosensor [40]. A precision converter for use with conventional multimeters was built by David L. Jones in 2010, but is no longer available [5]. A pre-amp circuit has the advantage of being low cost and easy to build.

LED was chosen as light excitation source because of its small size and low power requirements compared to incandescent light bulbs. Low power consumption also leads to less electromagnetic interferences. For the device constructed during this thesis, two types of 1 W LEDs were used: 1) UV spectrum LEDs at 365 nm and 2) visible spectrum "natural white" LEDs.

3. MATERIALS AND METHODOLOGY

3.1. Requirements for the device

The goal of this research project was to build and develop a device that could be used to measure a photocurrent generated by nanohybrid materials in the range of nanoampere. The amount of nanohybrid material to measure is between 1-2,5 mg, and the expected current for 1 mg of the nanomaterial was estimated to be around 150 nA.

The device must be able to do the following:

- hold a substrate with a sample of nanohybrids;
- illuminate the sample with UV and visible light;
- take a current reading from the sample.

The device should be practical and user friendly for routine use. It does not have to have very high accuracy, but it must be accurate enough to select promising nanomaterial candidates for or a more extended study.

3.2. Methodology

The process of measuring photocurrent generated from a nanohybrid sample is in principle simple: it must be deposited on a substrate with electrodes, excited with light and measured with a device capable of measuring the expected current. The mechanism through which HfO_2-CNT generates photocurrent is not in the scope of this thesis, but has been described in the articles published in 2016 and 2019 by P. Rauwel et al. [1], [36]. As described earlier, the problematic part is to measure nanocurrents and keep the noise minimal. It is theoretically possible to measure currents as low as the noise level [49]. The nanocomposites used to test the device were synthesized by Erwan Rauwel and Protima Rauwel.

3.2.1. Substrates

Comb electrodes etched from a circuit board were used because of their ease of fabrication, use and reusability. These electrodes were produced at EMÜ. Figure 4 shows the blueprint of the comb electrode. Line thicknesses of 0,25 mm, 0,30 mm and 0,35 mm were considered and 0,25 mm line with uniform 0,25 gap was selected for the measurement on the substrates.

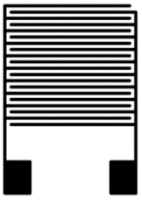

Figure 4. Blueprint of the comb electrode used for testing nanomaterials.

As an alternative, ITO-covered conductive glass was used as a substrate. Figure 5 shows the principle of the PV-cell prototype. The glass was cut into smaller pieces (2 × 3 cm) and two longer sides were covered with adhesive tape by 2 mm to keep a distance between the conductive layers (1). Metal clips were holding the glass pieces fixated (2). The nanohybrid sample is in between the glass pieces (3) and the glass pieces are shifted by 3 mm to allow connecting of measurement leads.

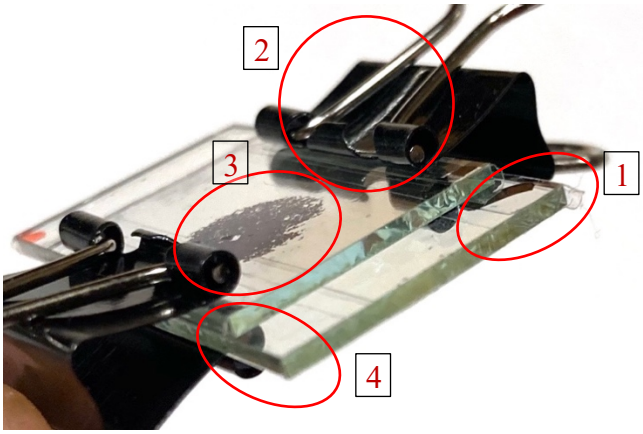

Figure 5. The principle of ITO glass-based PV-cell prototype. 1 – adhesive film holding glass apart; 2 – clamps fixating the glass; 3 – nanohybrid sample, 4 – glasses shifted by 3 mm to allow measurement leads to be connected.

Nanocomposites dispersed in ethanol solution were deposited on ITO-glass drop-by-drop in different amounts. The sample was left to dry at room temperature and then the sample was

weighed. For testing, another piece of glass was placed on top of the sample with the ITO side towards the nanohybrids, but the edges without adhesive tape 3 mm shifted so, that alligator clips of a DMM could be connected. The adhesive tape has an average thickness of 0,04 mm, so it keeps the ITO glass pieces apart, but enables the nanohybrid to conduct charges from one glass to another. On some samples an electrolyte solution was added between the glass and on other samples a layer of carbon was deposited on the second ITO glass. Alligator clips were used to fixate the substrate.

3.2.2. Light sources

UV and visible spectrum LEDs were used for light excitation of the sample. The power of each LED was 1 W and they were used in groups of three. The bandwidth of light and output were measured with a Gigahertz-Optik MSC15 light meter. During the evolution of the prototype, several configurations of LEDs were used: the first prototype had 3 UV LEDs and 3 visible light LED-s. From the second prototype 9 UV LEDs with reflectors and 3 visible LED-s were used and the last prototype had 9 of both types of LEDs. The UV LEDs were ordered at 365 nm wavelength but measuring with the light meter confirmed the actual wavelength of 371,6 ± 3,7 nm.

3.2.3. Measurement

A measuring circuit with a shunt resistor and an operational amplifier was used to amplify the photocurrent. Figure 6 shows the elementary diagram of that circuit and it contains a resistor R2 where a voltage drop occurs when current flows through the resistor. The operational amplifier amplifies that voltage drop and this is measured with a voltmeter or with a digital multimeter (DMM).

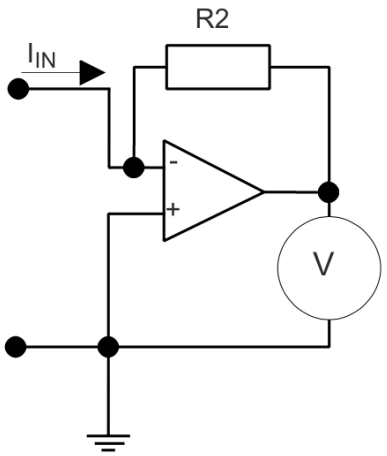

Figure 6. Elementary diagram of an operational amplifier-based measuring circuit [4].

The final circuit contains some additional parts (i.e. power regulators for the op-amp, adjustment potentiometer, range selection resistors etc.) and will be described in the results section.

3.3. Assembly of the device

Design of the device had to consider the following factors:

a) it has to be relatively compact, so it can be easily transported,
b) sturdy enough to travel in the luggage of an airplane.

Moreover, as the experiments continued, power supplies were moved further away from the measurement zone and the measurement part of the device was separated for noise reduction. Since the device needed to be as practical as possible, materials for building the prototypes were mostly chosen by availability in local electronics or home improvement stores. All the electrical components for the pre-amplifier were bought locally along with the boxes cables. Some locally unavailable parts like ITO glass and LED-s were ordered online from China.

3.4. Calibration of the device

Before a measurement circuit can be used, it needs to be calibrated. The initial plan was to calibrate the device with a semiconductor parameter analyser used in former studies on nanohybrids in the laboratory of IMEP-LaHC in MINATEC, University Grenoble Alpes,

France. The laboratory is equipped with sensitive precision measuring instruments for measuring photocurrent generated by nanostructures and is able to reliably measure current in nanoamperes and create I-V curves. The personnel at that laboratory also has experience in working with such hybrid nanocomposites.

A short study visit funding was approved by the Archimedes foundation's Kristjan Jaak short study visit programme, but the trip was delayed due to the Covid-19 outbreak. The preliminary calibration was done with the HoldPeak multimeter mentioned before. The work on the prototype will go on in PhD studies and the calibration is in perspective for the month of September as the availability of the scholarship was extended till the end of the year.

4. RESULTS AND DISCUSSION

4.1. Development

The development of the prototype was conducted in 3 stages.

1. The lighting part was constructed first and the resulting photocurrent from the selected samples was measured. This highlighted areas of improvement and triggered research to solve the problems that arose. At first the Hameg HM8112-3 precision multimeter was used to take readings from the samples instead of a conventional multimeter because of Hameg's higher resolution. The readings were unstable and it became evident that noise had to be reduced. Reducing the noise to acceptable levels required several steps of shielding and grounding.
2. In the next stage, a signal pre-amplifier was necessary to make the currents in nanoscale reliably readable for a DMM.
3. The final design and encasing were done at the last stage. In the paragraph below, all the changes to the prototypes are described.

Two multimeters were used while developing the device: HoldPeak HP-39C and Hameg HM8112-3. HoldPeak HP-39C is a 3¾-digit 6000 count handheld DMM with a DC current resolution of 0,1 μA [50]. Hameg HM8112-3 is a 6½-digit 1,2M-count desk precision-DMM with a DC current resolution of 1 nA [51].

4.2. Prototypes

4.2.1. Prototype 1

The first prototype was made as a proof of concept of the lighting part of the device. It contained 3 UV and 3 visible light LEDs in a circular pattern, separately switchable. Underneath the lights was a box with the power supplies for the LEDs and switches. There was no shielding or grounding. Measuring was done directly with a multimeter. Figure 7 shows the first prototype measuring a PV cell with the HoldPeak multimeter. One important downside of this prototype was, that the operator had to hold the multimeter leads to keep the substrate in place causing interference while doing so.

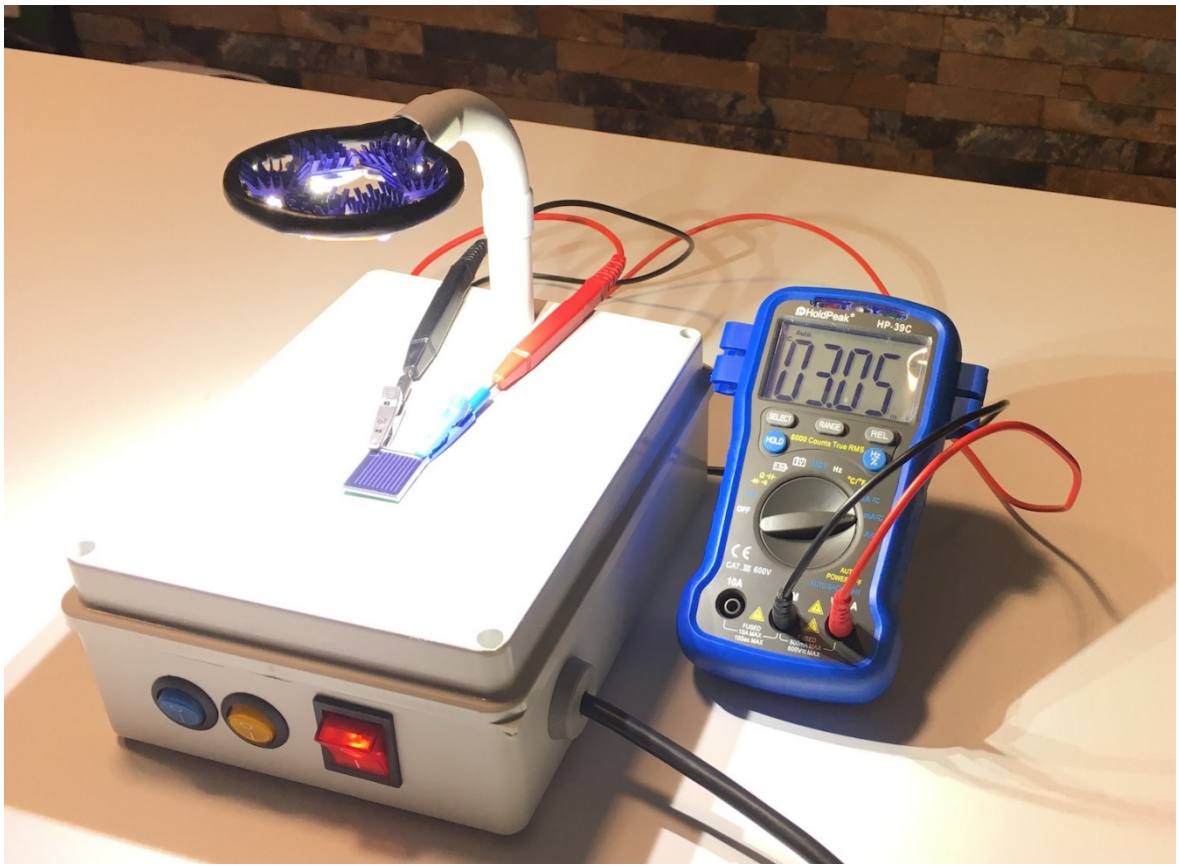

Figure 7. Prototype 1 with lights on and a factory solar cell sample being measured.

The first photocurrent measurements showed that shielding is imperative for all measurements. The reading was fluctuating and the noise level was around 50 nA.

4.2.2. Prototype 2

The second prototype increased light output and gave an improvement in noise reduction. It had 3 groups of UV LEDs in 3-LED reflectors and 3 visible light LEDs in a circular pattern. A metal ring was added around the lights in an attempt to shield the interference from the LED wiring. The power supplies had a basic shielding in the form of tin foil and the wires to LEDs were grounded. Another important upgrade was adding a substrate holder out of alligator clamps, which was attached to the base under the light. The alligator clamps were holding the substrate with the sample in place while measurement leads of the Hameg multimeter were connected to the clips. Other than that, the configuration remained the same as the first prototype. Measurements were done directly with a multimeter. Figure 8 shows

a sample with the second prototype. Folded paper was placed under the substrate to keep it levelled.

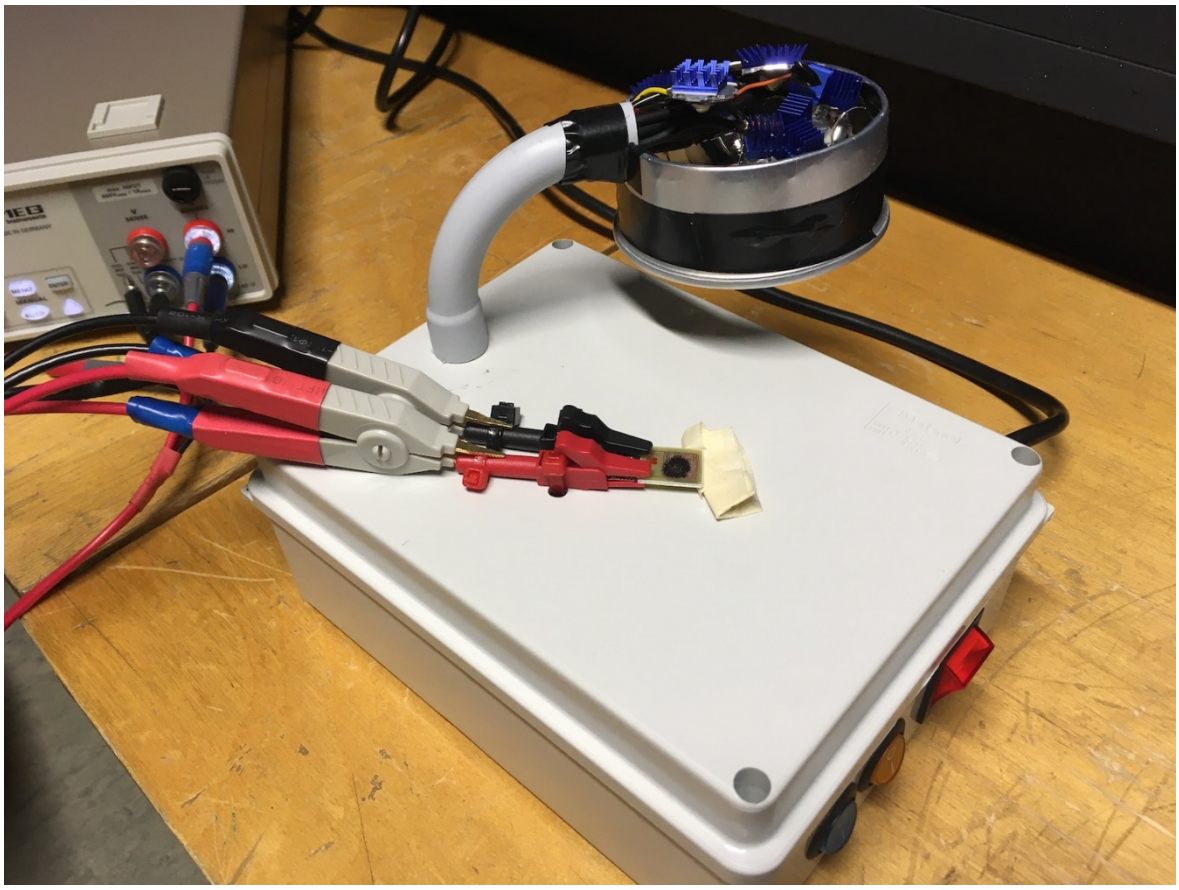

Figure 8. Prototype 2 setup with nanocomposites spread on comb-electrode substrate.

The measurements showed that shielding was efficient and a photocurrent was detectable, but the shielding still needed improvement, because noise level was still about 28 nA, which was too high for such measurements.

4.2.3. Prototype 3

The third prototype was primarily a test object for the measurement circuit (pre-amplifier) with an operational amplifier. To decrease noise, the power supply cable to the lighting unit was replaced with a 3-meter shielded and grounded cable. The lighting part remained the same. It had 3 groups of UV LEDs in 3-LED reflectors and 3 visible light LEDs in a circular pattern. The reflectors purpose was to concentrate the light into a beam. Figure 9 shows the pre-amp circuit in testing.

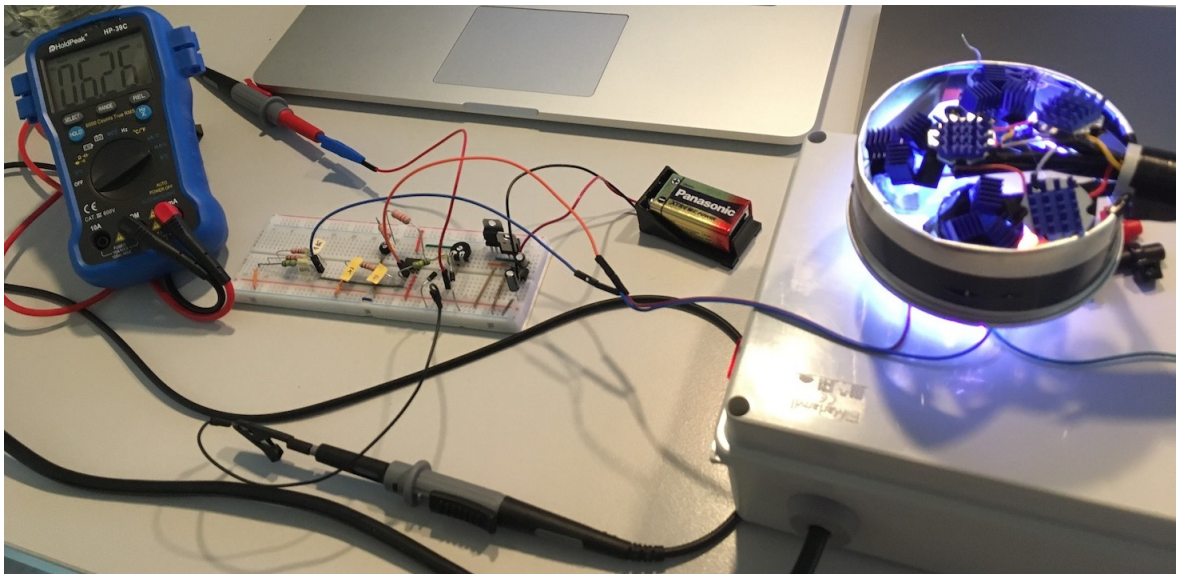

Figure 9. Prototype 3 with pre-amp circuit being tested with UV light.

No testing of photocurrent generation was done with the third prototype because the prototype was quickly updated to next version to reduce noise.

4.2.4. Prototype 4

Based on previous prototypes tested, the fourth prototype had a new design for the lighting unit. Its support was out of convex shaped perforated metal that helped to concentrate the light to one area. It had 9 UV and 9 visible light LEDs in a circular pattern. 6 visible light LEDs were not connected to a power supply, but were planned to be connected in the next stage. The LEDs were glued to the top of the metal convex to keep the wiring of LEDs on the other side of the sample and the measuring part. The metal support acted as a shield from electromagnetic interference and helped to direct the interferences in the opposite direction from the sample. Figure 10 shows the setup of prototype 4. The measurement circuit was still on the breadboard, because a suitable switch for choosing the range (switch S1 in Figure 11) was unavailable. The pre-amp circuit was placed in a temporary metal box for shielding and longer probe cables were twisted around each other to mitigate interferences.

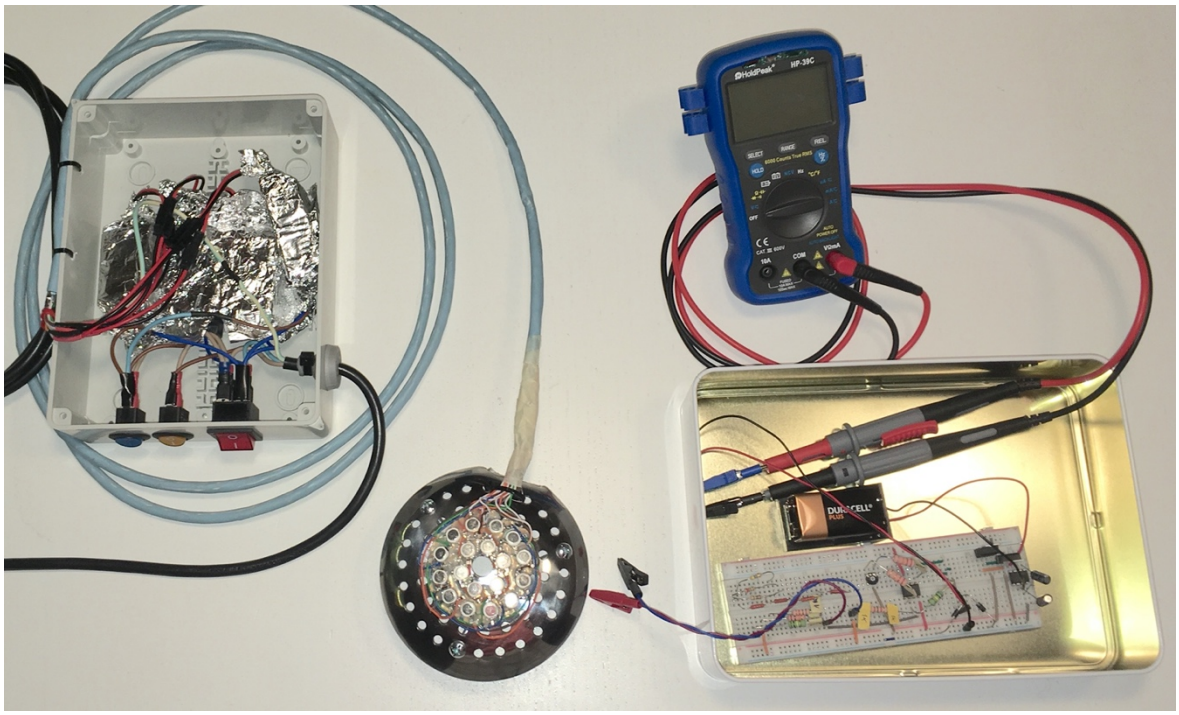

Figure 10. Prototype 4 with HoldPeak multimeter.

Testing showed that using a longer cable between the light and the power supplies, the metal reflector and housing the pre-amplifier in a metal box reduced the noise to an acceptable level of under 2 nA.

The shortcomings of this prototype were:

- A better cable for the lighting unit is required. Currently the noise level changes when the operator is too close (1-2 cm) to the cable. One with better shielding should be used.
- The wiring of the LEDs must be enclosed in a metal part or a faraday cage. Currently the electromagnetic (EM) noise is reflected away from the measuring area, but it is still dispersing and finding its way to the measurements.
- As the powerful LEDs get hot when lit, the glue currently used will get soft and the LEDs may move out of their intended position. A cooling solution and a more suitable glue should be considered for the LEDs.
- The power supplies and the measurement pre-amp should be mounted into a permanent shielding box of a suitable size for better usability.
- The pre-amplifier circuit should be finalized and built onto a circuit board or a stripboard.

4.2.5. Further development of the prototype

Table 1 shows a summary of the previous development of the prototypes and planned upgrades for the fifth version.

Table 1. Properties of different prototypes

Property	Prototype number				
	#1	#2	#3	#4	#5*
Number of UV LEDs	3	9	9	9	9
Number of visible light LEDs	3	3	3	3	9
Measurement amplifier	-	-	breadboard pre-amp	breadboard pre-amp	stripboard pre-amp
Measurement device	Hameg DMM	Hameg DMM	HoldPeak DMM	HoldPeak DMM	micro-controller
Noise background (nA)	50 (unstable)	30	-	2	*
Power supplies	2	4	4	4	5
Shielding	none	power supplies	power supplies	power supplies LEDs LED cable Pre-amp	power supplies LEDs LED cable Pre-amp Switchbox
Casing material	plastic	plastic	plastic	plastic/metal	metal

Remarks. *The fifth prototype was not completed by the time this manuscript was finished.

The fourth prototype achieved most of the goals set for the device but there were several aspects (outlined in the previous section) that could be improved. Most importantly the pre-amp should be built onto a stripboard and the setup should be firmly fixed into enclosures. Additional improvements not mentioned above are:

1) add one power supply to power the 6 visible light LEDs, which are currently not used;
2) replace the multimeter with a microcontroller with display and memory card support. By removing the leads to the DMM the noise should go down some more and a memory card would allow storing the reading to be processed later;
3) construct a holder which is compatible with ITO glass substrates.

4.3. Measurement pre-amplifier

The pre-amplifier schematic was built around a TL081 general purpose Junction Field Effect Transistor (JFET) single operational amplifier. Figure 11 displays the schematics of the pre-amp circuit and (A) its power supply circuit (B). Figure 12 below shows the circuit on a breadboard.

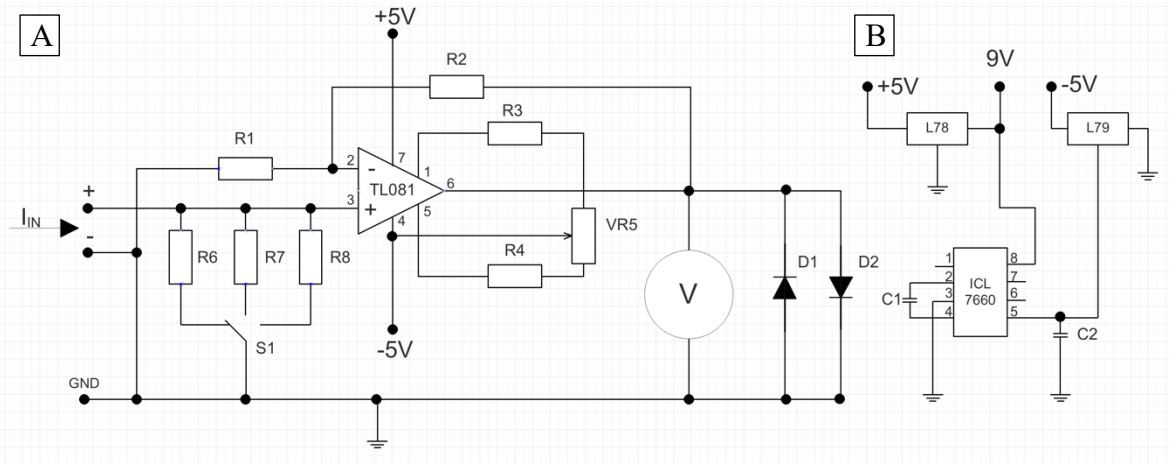

Figure 11. Schematics of (A) the measuring circuit with operational amplifier and (B) its power supply [5], [52]–[56].

The current to be measured will be connected to the + and - connectors (Figure 11A). Applying a current will result in a voltage drop on resistor R2 which will be amplified by the TL081 operational amplifier. That voltage will be measured with a voltmeter or a DMM between the op-amp output and the virtual ground. The diodes in parallel with the voltmeter are there to protect the circuit from overcurrent. The resistors R6, R7 and R8 are range selection resistors which are selected with a 3-position switch SW1. The circuit with R3, R4 and VR5 is the offset to zero adjustment part. Adjustment is done with variable resistor (varistor) VR5.

Figure 11B is the power circuit for the operational amplifier. It is powered by a 9 V battery. Although the operational amplifier would accept 9 V voltage, the voltage is regulated because a battery will discharge over time and that would affect the measurement. 5 V supply voltage was chosen for the amplifier, because it is a common voltage available from many sources and it is easy to convert other voltages to 5 V. Here, a L78 positive and a L79

negative voltage regulator are used. The L79 negative voltage regulator needs negative voltage as input, so an ICL7660S voltage inverter is used to invert the input voltage.

An important property of an amplifier is its gain. It shows how many times the input to the amplifier is multiplied. The gain of a non-inverting amplifier circuit is calculated by dividing the shunt resistance *R2* with the resistance of *R1* and adding a constant 1. The formula and a theoretical calculation, if *R2* = 100 kΩ and *R1* = 1 kΩ. is as follows [5], [56], [57]:

$$gain = 1 + \frac{R2}{R1} = 1 + \frac{100000}{1000} = 101 \quad (2)$$

That means that the gain of the pre-amplifier circuit is 101, provided the actual resistors have the said resistance. After measuring, the actual resistors have resistances of:

R1 = 0,992 kΩ

R2 = 98,6 kΩ

and the calculated gain equals:

$$gain = 1 + \frac{98600}{992} = 100{,}40$$

The actual gain of the pre-amplifier is *gain* = 100,4. Knowing the actual gain based on the resistors used helps to calibrate the measuring circuit.

Figure 12 displays the pre-amplifier circuit on a breadboard with major components pointed out: 1 – operational amplifier;

2 – voltage inverter;

3 – positive voltage regulator;

4 – negative voltage regulator;

5 – resistors;

6 – diodes;

7 – capacitors.

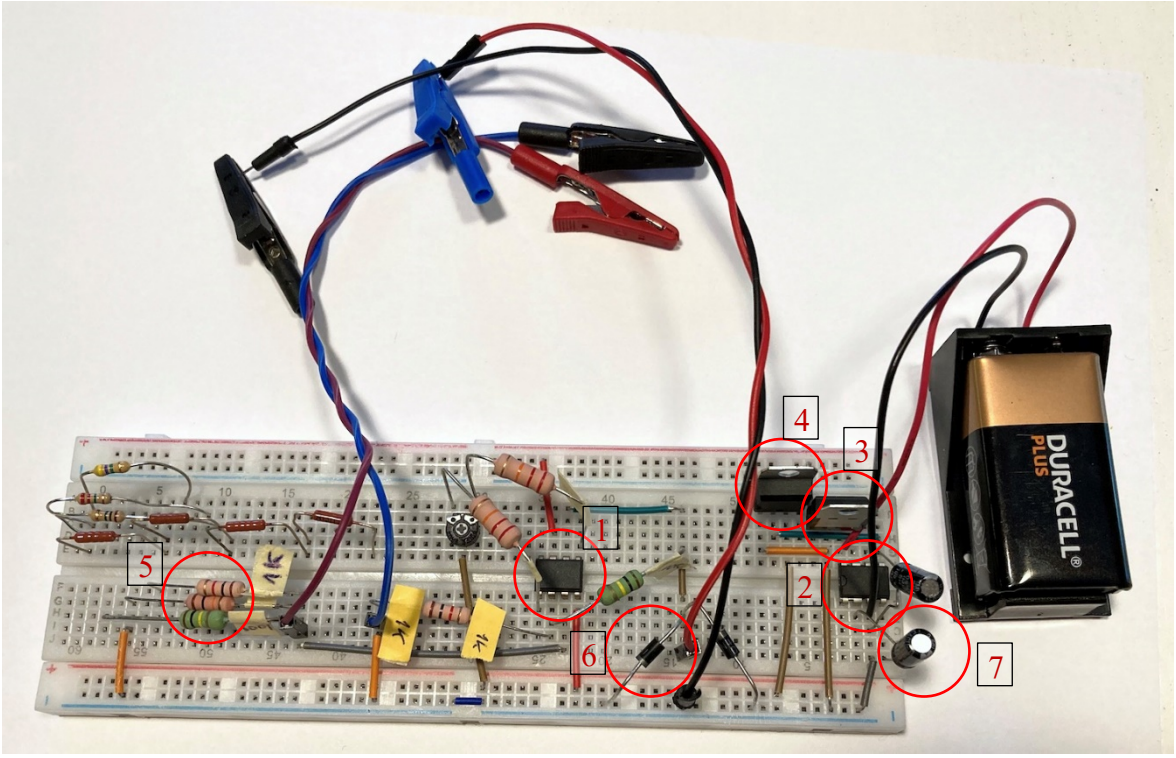

Figure 12. The pre-amplifier on the breadboard: 1 – operational amplifier; 2 – voltage inverter; 3 – positive voltage regulator; 4 – negative voltage regulator; 5 – resistors; 6 – diodes; 7 – capacitors.

Table 2 shows the specifications of the components in the displayed circuits (Figure 11 and Figure 12). A description of the parts follows below.

Table 2. Components and specifications of the pre-amplifier circuit

#	Type	Specification	Marking	Values	Count
1	Operational amplifier	TL081CN	TL081	-	1
2	Voltage inverter	ICL7660SCPAZ	ICL7660	-	1
3	Positive voltage regulator	UA78S05-ST	L78	-	1
4	Negative voltage regulator	UA7905-MBR	L79	-	1
5	Resistors		R1, R6	1 kΩ	2
			R2, R8	100 kΩ	2
			R3, R4	22 kΩ	2
		variable resistor	VR5	5 kΩ	1
			R7	10 kΩ	1
6	Diodes	1N4007	D1, D2	-	2
7	Capacitors	22/16PHT	C1, C2	22 µF	2

Description of the parts:

1) Operational amplifier TL081CN.

TL081CN is a high-speed JFET (Junction Field Effect Transistor) single input operational amplifier. The one used here is in DIP8 package, as seen on Figure 11 A. An operational amplifier has differential input (+ and -) and produces an output potential that is much larger than the input.

2) Voltage inverter ICL7660SCPAZ.

A voltage converter can perform different tasks with voltage, such as divide, double and invert. The latter is the task it is required in this schematic. It requires two external capacitors to function well and this is also in DIP8 package.

3) Positive voltage regulator L78S05CV.

Voltage regulators take higher voltage as input and output a defined voltage. The ones used here take up to 35 V and output 5V.

4) Negative voltage regulator L7905CV.

Voltage regulators are separate for positive and negative voltages. This one is for negative voltages, but other than that similar to the previous one. Both are in TO-220 packages.

5) Resistors 1k, 5k, 22k, 10k, 100k.

Resistors are probably the most common electronic parts, used for limiting and dividing current among other uses. Resistor is a passive component. A variable resistor or a potentiometer is such resistor that can be adjusted to one's needs. In this circuit, it is used to adjust the measurement reading to zero if needed.

6) Diodes 1N4007.

The main purpose of diodes is to block current flow in one direction, but they can also be used to protect circuits from too high current.

7) Capacitors 22/16PHT 22 μF.

Capacitors are used to store energy in an electric field. In this circuit they are used by the voltage converter.

The listed parts were all purchased locally in Estonia. The resistors purchased were the most affordable products, with precision of 5 %. If a post-prototype device is constructed, resistors with higher precision of 1 % or 0,1 % and low temperature coefficient should be chosen [5].

4.4. Lighting

The lighting part of the prototype (Figure 10) consists of two parts: a) a box with power supplies and switches; b) the lighting unit with LEDs and their holder. Figure 13 shows the recent lighting unit from the side (A), from where the wiring is visible and from the bottom (B) from where the LED-s are visible. The LED holder is made of a convex shaped perforated metal, where the holes had to be drilled bigger to fit the LEDs.

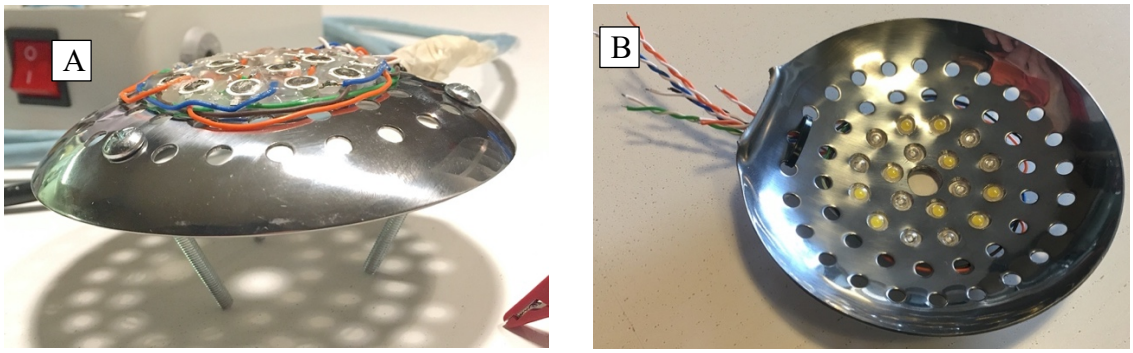

Figure 13. Lighting unit: A – from the side; B – from below.

Table 3 displays the parts used in the prototypes. A description of the parts follows below.

Table 3. List and specifications of building parts of the device

#	Type	Specification	Count
1	1-watt UV LED	365 nm	9
2	1-watt visible light LED	"natural white"	9
3	LED power supply type 1	280-300 mA constant current	4
4	LED power supply type 2*	350 mA constant current	1
5	Cable	Cat6 F/UTP	3 m
6	Box	150 × 200 mm	1

Description of the parts:

1) 1-watt UV LED (Figure 14A).

A light emitting diode is a well-known electronic component. With 1-watt power it is sometimes called a Power LED, although there are more powerful ones available nowadays. The UV LED was sold with a nominal wavelength of 365 nm, but the measurements showed a peak wavelength of 372 nm.

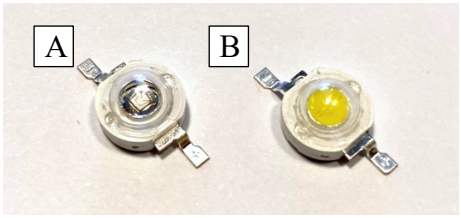

Figure 14. LEDs used for lighting: A – UV LED; B – visible spectrum LED.

2) 1-watt visible light LED (Figure 14B).

Principally the same as the UV LED but emanating in the visual spectrum. LEDs have a fixed voltage and current requirement. The LEDs used here work on 3,2-3,4 V and up to 350 mA.

3) LED power supply type 1 (Figure 15).

This is a basic constant current power supply for the LEDs mentioned before. It works with 1 to 3 LEDs and regulates the voltage based on its load. The nominal output is 280-300 mA.

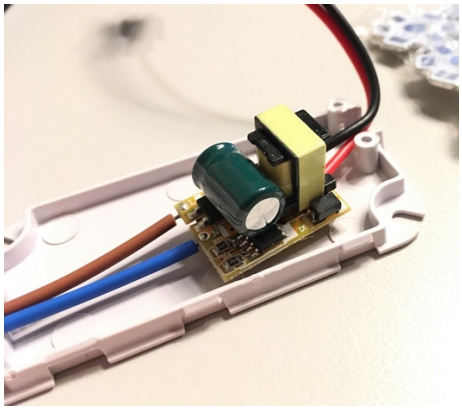

Figure 15. Constant current power supply for 1-3 LEDs without its cover.

4) LED power supply type 2 - MeanWell APC-12-350 (Figure 16).

This is a more powerful and advanced constant current power supply. The output is 350 mA and it can support 3-10 LEDs.

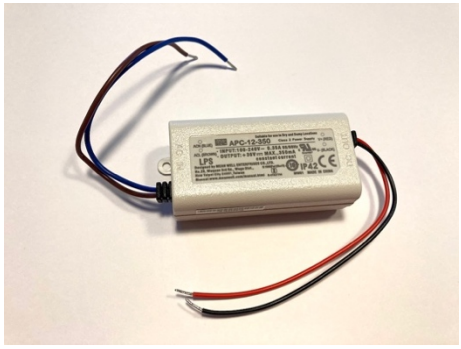

Figure 16. Constant current power supply for 3-10 LEDs.

5) CAT6 U/FTP cable.

A shielded computer network cable was used for the power cable to the lighting unit. It was chosen because it was known shielded cable with 8 wires, which was perfect for supplying power from 4 power supplies. The wires inside this cable are twisted in pairs and each pair is wrapped in tin foil shielding.

6) Box 150 × 200 mm

A plastic box was used to hold the power supplies. Initially it was planned to double as light and substrate holder, but the electromagnetic noise emanating from the power inverters made that impossible.

Light used for sample excitation was measured with a Gigahertz-Optik MSC15 light meter. The light meter returns a variety of measurements, but the relevant parameters to this prototype were spectrum distribution and light intensity per 1 m^2. Figure 17 below displays the spectrum on UV (blue line) and visible light (green line) LEDs. This light meter is a B-class device with 1 % accuracy [58].

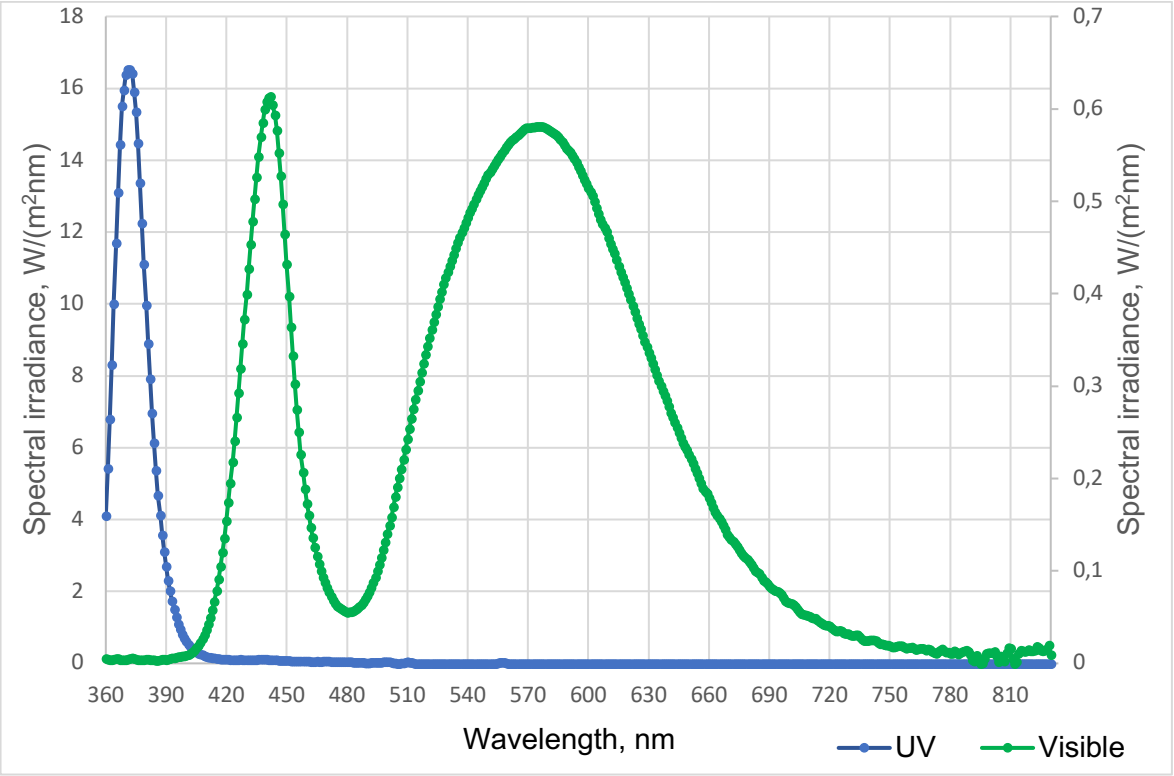

Figure 17. Spectral irradiance and wavelength of the LEDs used in the prototypes: Blue line – UV LEDs on primary Y-axis, green line – visible light LEDs on secondary Y-axis.

Measurements were taken from a distance of 50 mm, which is the distance of the sample from the light source. Irradiance of 9 UV LEDs was 339 W/m^2 and of 3 visible light LED-s 95,23 W/m^2. UV light was strongest at 372 nm (average of 5 measurements) wavelength, which is 7 nm higher than that in the specifications. The visible light LED-s show two peaks, one at 441 nm, the other at 575 nm.

The wavelengths calculated from the Tauc plot (Figure 3) in paragraph 2.5, that fall into the range of visible light, were λ_1 = 459,20 nm and λ_2 = 399,95 nm. The UV LED's peak of 372 nm is below λ_2. This means that the UV LEDs are suitable based on the plot. The visible light LED has a strong spike at 441 nm which is lower than λ_1, but the major amount of light is from 510 nm to 660 nm, where the nanohybrid does show less absorbance. Based on the plot, cooler and lower wavelength LEDs should be used if higher yield is desired.

The solar panels are tested with an illumination of 1000 W/m^2 according to IEC 61215 standard. 9 watts of UV LEDs gave an output of 339 W/m^2. It is noteworthy to mention that 9 W of LED light can cover 1/3 of the standard illumination required for testing. Three times

as much LEDs would be required to reach 1000 W/m^2 (339 · 3 = 1017) or alternatively, 3-watt or stronger LEDs could be used to keep the number of LEDs lower. Heat generation must be considered when using more LEDs.

The most challenging part about lighting was to find a suitable support for the LEDs. Initially reflectors were used which worked well from lighting perspective but provided no shielding from interferences. Finally, a convex shaped perforated metal support was found which required little modification, provided sufficient reflection and isolated the interferences of the wiring from the area where measurements would be made.

4.5. Substrates

A substrate is a base upon which a sample is deposited on. Comb electrodes were chosen for this purpose in this setup, because they are easy to make, reusable and sturdy. The comb electrodes were made in December 2019 in EMÜ. Figure 18 shows the etching process of the circuit boards. Two circuit boards were made, one with 4 and the other with 6 electrodes. The board with 6 electrodes did not succeed because of too long heating time which left the electrodes short-circuited. Out of the other board, 3 substrates were usable.

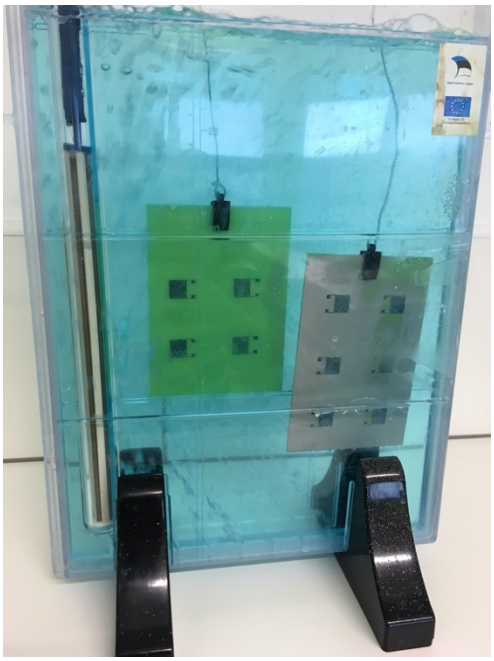

Figure 18. The copper substrates in the etching process.

Figure 19A shows the three resulting substrates with a nanohybrid sample deposited on them. The substrates are numbered 1-3. Figure 19B shows ITO glass substrate with a 1 drop sample of HfO_2-CNT nanocomposite and sides covered with adhesive tape. The samples in all 3 cases were spread differently on the comb electrode.

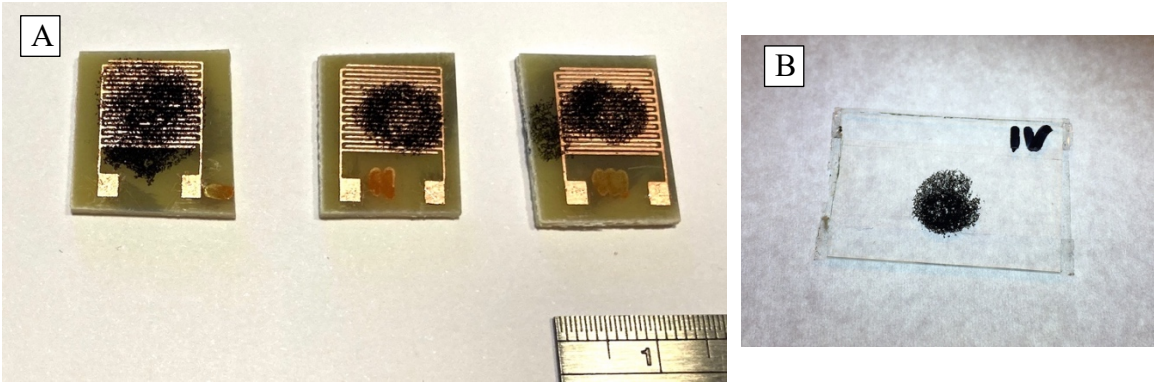

Figure 19. Substrates: A – copper substrates 1, 2 and 3 with a HfO_2-CNT nanocomposite samples; B – ITO glass substrate with a 1 drop sample of HfO_2-CNT nanocomposite and sides covered with adhesive tape.

ITO glass was chosen, because it has a conductive indium-tin oxide coating. Figure 20 shows the data sheet of ITO glass provided by its seller, where the thickness of that layer can be found. As the purchased glass has a 10 Ω specification, the ITO layer thickness is 185±20 nm. Using that conductive layer, it can be used to simulate a PV-cell or it can be used as a substrate where the sample is less exposed to air.

Performance specifications of ITO conductive film layer				
specification	SQ（Ω/□）	Transmittance(%)	Etching time/s	ITO film thickness
500Ω	350-500Ω	≧90	≦30	120Å ±30Å
150Ω	100-150Ω	≧87.0	≦30	150Å ±30Å
100Ω	80-100Ω	≧87.0	≦40	230Å ±50Å
80Ω	60-80Ω	≧86.0	≦45	300Å ±50Å
60Ω	40-60Ω	≧85.0	≦60	350Å ±50Å
50Ω	40-50Ω	≧84.0	≦65	400Å ±50Å
40Ω	30-40Ω	≧85.0	≦70	500Å ±100Å
30Ω	20-30Ω	≧80.0	≦100	650Å ±100Å
20Ω	10-20Ω	≧85.0	≦140	950Å ±100Å
17Ω	15-20Ω	≧85.0	≦180	1350Å±150Å
15Ω	10-15Ω	≧85.0	≦180	1350Å±150Å
10Ω	6 -10Ω	≧84.0	≦240	1850Å±200Å
7Ω	5 - 7Ω	≧82.0	≦350	2200Å±300Å
5Ω	3 - 5Ω	≧77.0	≦400	3500Å±300Å
可订做厚度：0.33-2.0MM；（特殊厚度可以商议订做）				
可订做规格：6*6MM-355.6*406.4MM				

Figure 20. Specifications of the purchased ITO glass sheets [59].

Figure 21 shows ITO glass-based sandwiched substrates. A – one drop of HfO_2-CNT, B – one glass area covered with HfO_2-CNT, the other glass area covered with carbon spray. The glass is placed with ITO layers facing eachother, with a 3 mm offset on the sides where the measurement clamps can be connected. The long sides of the glass are covered by 2 mm with a layer of polyimide tape tape, which will keep the glass pieces from contact (short-circuit).

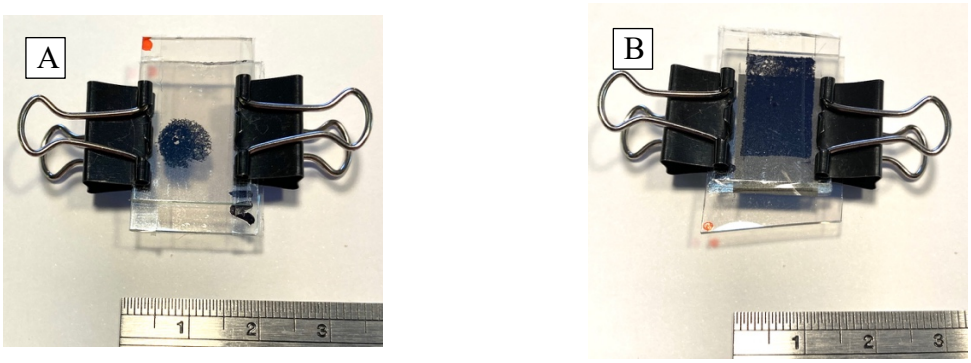

Figure 21. ITO-glass pieces sandwiched together: A – only HfO_2-CNT sample; B – HfO_2-CNT sample on one glass and carbon spray on the other side.

The ITO glass substrates are more difficult to prepare and handle than the comb electrode substrates. The most challenging part has been to design a holder for these for illumination. The current prototype does not have a suitable holder, but one for the next build is planned.

4.6. Measurements

4.6.1. Calculation of accuracy

The accuracy of the measurement depends on the precision of the pre-amplifier and of the digital multimeters used. The ambient temperature is another factor to be considered in measurements – the devices are meant to be used at room temperature and temperature fluctuations will reduce the accuracy. In the pre-amplifier circuit, the accuracy and temperature coefficient of resistors define the precision. The accuracy of multimeters is found in the user's manual. Table 4 displays the relevant specifications of the used multimeters. Figure 22 shows the used multimeters: A – HoldPeak HP-39C; B – Hameg HM8112-3. As seen from the table, the Hameg precision multimeter is capable of measuring nanocurrent directly, but HoldPeak will need a pre-amplifier. The measurement from the output of the pre-amplifier will be taken in millivolts, because the operational amplifier is amplifying a voltage drop, as described earlier.

Next, the accuracy of a measurement is calculated, assuming a reference current of 20 nA. The accuracy of the pre-amp circuit is dependent on the accuracy of the shunt or range resistors R6, R7, R8 [5]. The available resistors had a precision of 5 %, so the resulting accuracy is >5 %. Resistors with better precision (1 % or 0,1 %) are available on order. The temperature coefficient will not be regarded, as this is in the magnitude of 10^{-4} Ω/°C for a 5 % resistor [60] and 10^{-5} Ω/°C for a 1 % precision resistor [61].

Assuming the current to be measured is 20 nA, a 5 % accuracy results in an uncertainty of:

$$I = 20\ \text{nA} \cdot \frac{5}{100} = 1\ \text{nA}$$

This means that the actual reading at the pre-amp output is between 19 nA and 21 nA. Using 1 % resistors would increase the pre-amp circuit accuracy to ± 0,2 nA and 0,1 % resistors to 0,02 nA.

Table 4. Specifications of used digital multimeters

	HoldPeak HP-39C [50]	Hameg HM8112-3 [51]	
integration time	-	0,1 s	1-60 s
digits	3¾	6½	
counts	6000	1200000	
mV range	600 mV	100 mV	
mV resolution	0,1 mV	1 µV	0,1 µV
mV accuracy	± (0,5 % + 2 digits)	0,005 % + 0,0006 %	
mV impedance	>100 MΩ	>1 GΩ	
µA range	600 µA	100 µA	
µA resolution	0,1 µA	1 nA	0,1 nA
µA accuracy	± (1,2 % + 2 digits)	0,02 % + 0,002 %	
burden voltage	N/A	< 600 mV	

The HoldPeak DMM can't measure nanoamperes directly, so the output of the pre-amplifier will be measured. The accuracy of the millivolt range is given in the manual as ± (0,5 % + 2 digits), which means ± 0,5 % of the reading + 2 last digits of the display at resolution of 0,1 mV. Assuming the pre-amplifier output gives a reading of 20 mV, the calculation is as follows:

$$U = 20\ \text{mV} \cdot \frac{0{,}5}{100} + 0{,}2 = 0{,}3\ \text{mV} \qquad (3)$$

This means, that the actual reading of the multimeter is between 19,7 mV and 20,3 mV. Adding these results to the pre-amplifier's result gives a low value of 19 - 0,3 = 18,7 mV and a high value of 21 + 0,3 = 21,3 mV. The resulting ± 1,3 nA precision is acceptable considering the low price of this setup compared to the high price of the professional Hameg multimeter. By changing the resistors to ones with 1 % accuracy, the precision can be increased to ± 0,7 nA and with better resistors even more.

A

B

Figure 22. Digital multimeters used for measuring: A – HoldPeak HP-39C [50]; B – Hameg HM8112-3 [51].

The Hameg precision multimeter makes the error calculation easy by giving an accuracy percentage in the user's manual, which already includes all the parameters. For the micro-ampere range it is 0,02 % + 0,002 %. The first percentage is the measurement accuracy; the second one is temperature dependant. The given value represents the normal temperature of 23 ± 2 ºC. The calculation is simple, since the Hameg can measure 20 nA directly:

$$I = 20\ \text{nA} \cdot \frac{0{,}02}{100} + 20\ \text{nA} \cdot \frac{0{,}002}{100} = 0{,}0044\ \text{nA} \qquad (4)$$

This means, that the actual reading is between 19,9956 nA and 20,0044 nA, which is very accurate compared to handheld consumer digital multimeters.

4.6.2. Calibration

As mentioned before, it was planned to calibrate the device in Grenoble but that was not possible. A preliminary calibration was done with the HoldPeak multimeter. The first calibration was done on 26.04.2020 but that did not give the expected results. Later, an error was found in the pre-amplifier circuit and the calibration had to be re-done on 17.05.2020. The procedure involved creating a known nanocurrent and measuring this nano-ampere current directly with the digital multimeter and through the pre-amplifier.

As the power source, two Sanyo Eneloop rechargeable batteries were used with a series connection voltage of 2,56 V. The voltage was measured in the beginning and at the end of the measurement process and no power drop was observed. The nanocurrent was generated by connecting a resistor to a power source by one contact and connecting the multimeter or the pre-amplifier to the other contact and to the other terminal of the power source.

Figure 23 shows the resistors on a breadboard in the setting they were used for calibration. Table 5 shows the results of the calibration. The first column shows the nominal resistance of the resistors used for calibration and the second column is the measured resistance of same resistors. The third column shows the current measured with the HoldPeak multimeter and the fourth column shows the current calculated by Ohm's law (example below). The last three columns are the values displayed on the multimeters screen when measuring in the millivolt range. The range choice resistors are resistors R6, R7 and R8 on Figure 11A, used for choosing the measuring range of the pre-amplifier. It is visible from the table, that the

first range works for all readings, but with a resolution of 1 nA. The 10 kΩ resistor has a 0,1 nA resolution and the 100 kΩ resistor has a 0,01 nA resolution.

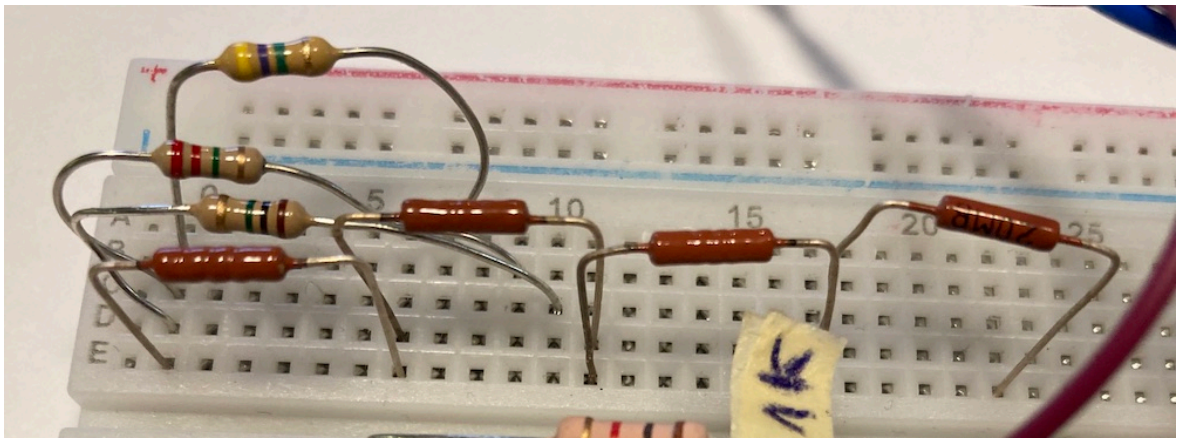

Figure 23. Resistors used for calibration on a breadboard.

When doing measurements, the ambient temperature has to be considered. While doing these measurements and calibrations, the ambient temperature was the same on all occasions.

Table 5. Calibration results

Nominal resistance	Measured resistance	Directly Measured current	Calculated current	Range choice resistors		
				1 kΩ	10 kΩ	100 kΩ
MΩ	MΩ	µA	nA	Measured value after pre-amplifier, mV		
1	0,989	2,6	2588,47	260,7	-	-
2,2	2,152	1,1	1189,59	119,4	-	-
4,7	4,760	0,5	537,82	53,1	541,6	-
20	18,75	0,1	136,53	13,2	138,0	-
2 × 20	38,30	0	66,84	6,3	67,4	677,0
3 × 20	56,10	0	45,63	4,3	46,3	467,7
4 × 20	74,10	0	34,55	3,1	35,1	353,3

As the results show, the readings from the range resistors are off from the calculated current. That is resulting from the fact, that the resistors are of 5 % precision. Using more precise resistors would give better results. Additionally, a coefficient can be found for each resistor and taken in account when processing results. Last, a better multimeter should be used for calibration, for example the Hameg should be sufficient for calibrating by the resistors.

4.6.3. Photocurrent

The photocurrent measurement was done to confirm that the setup was able to measure the nanocurrent once the sample was excited with light. Table 6 shows the results from photocurrent measurements with comb electrode substrates. Figure 24 is visualization of the data from Table 6.

Table 6. Photocurrent and noise measurement results with comb electrode substrates.

Device	Prototype 1	Prototype 2	Prototype4
Noise, nA	50	41	1,7
Substrate #1, nA	20	7	2,3
Substrate #2, nA	20	7	1,4
Substrate #3, nA	-	4	1,9

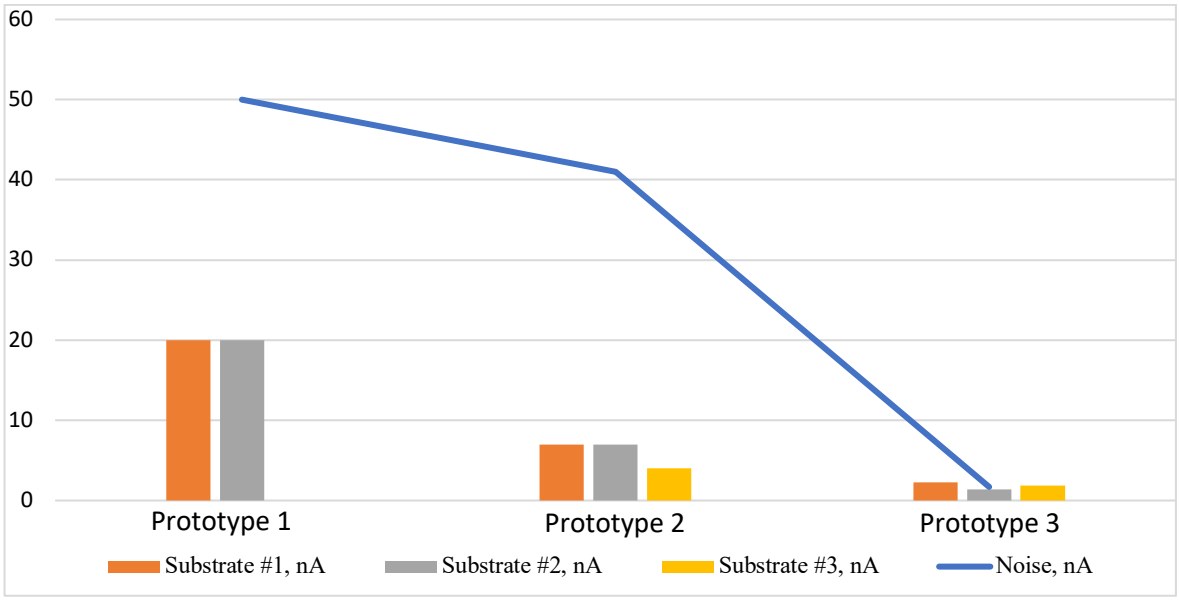

Figure 24. Measurement results and noise

Tests with prototype 1 were performed on 05.02.2020. Hameg HM8112-3 multimeter was used. Tests gave an approximate result of 20 nA of current with 3 W UV LED photo-excitation. As the measurement fluctuating, strong electromagnetic interference was suspected and 20 nA photocurrent generation was considered too high for 3 W photoexcitation. The general noise floor was 50 nA. Sandwiched ITO glass was tested as well, but no usable results were achieved. There was no noticeable difference between a nanohybrid-ITO sample and a plain ITO-glass sandwich, possibly due to noise.

Tests with prototype 2 were performed on 17.02.2020. Current generated by light excitation was measured at 7 nA with the Hameg HM8112-3 multimeter. Due to the shielding, the measurement was not fluctuating anymore, and noise was somewhat lower but so was the photocurrent. Nevertheless, this result seemed plausible. ITO glass was not tested, because no suitable holding method had been found.

Third testing with the fourth prototype was carried out on 17.05.2020. The third prototype was skipped because it was quickly upgraded to fourth version. On one side, the efforts on noise mitigation had paid off, as the noise has gone down to below 2 nA. Interestingly the nanocurrent generated by the samples had also gone down. ITO glass was not tested, because no suitable holding method had been found.

5. SUMMARY AND CONCLUSION

The main objective of this master's thesis was to develop a prototype setup combining light excitation (UV and visible light) and measurement of the photocurrent exhibited by hybrid nanocomposites (i.e. HfO_2-CNT) developed by the research group. Additionally, it was necessary to select a test substrate that would hold the nanohybrid sample. The challenging part was measuring the very small amount of current generated by these nanocomposites, which was expected to be in the range of nano-ampere. The purpose of this setup was to enable scientists to routinely study the hybrid nanocomposites with sufficient accuracy to identify the most promising materials for further research.

Literature was reviewed to understand what has been done previously to develop such measurement devices. In general, expensive specialized equipment is used, but no portable device of similar purpose was further developed. One device that could be used for measuring IV-curves for PV-cell prototypes was identified, but that device did not include the light excitation part.

During the development of the setup, four waypoints or separate prototypes were developed. Each new one was an improvement to the previous prototype developed, and at the same time, new challenges appeared that needed to be solved with another prototype. One of the main aspects of improvement through all the prototypes was shielding the surrounding interferences and mitigating the noise from the measurement. Finding a suitable holder and reflector for the LEDs was the second major unexpected difficulty for such development.

To measure the nanocurrent, a pre-amplifier circuit was constructed, with a possible resolution of 0,01 nA. The noise mitigation was successful. When the first protype exhibited a noise floor of 50 nA, the last prototype exhibited a noise background of only 1,7 nA with identified areas for further improvement. The main drawback in the process was the Covid-19 outbreak during spring 2020. That delayed both the research and the laboratory visit to France. During the short stay, it was planned to calibrate the developed setup with precision measuring equipment in Grenoble, but less accurate methods had to be used instead.

Fortunately, the scholarship was extended until the end of the year and the next plan is to complete the calibration later during PhD studies.

As a result, a measurement setup prototype was developed that is able to measure nano-ampere current with reasonable accuracy and low noise floor. With 9 UV LED's its lighting power is 339 W/m^2 and it was confirmed that comb electrode substrates on circuit boards work for harvesting the photocurrent generated by hybrid nanocomposites. Areas with possibilities of further improvement have been identified and detailed steps of improvement are provided that would make it possible to take the setup out of prototype status.

LITERATURE

[1] P. Rauwel, A. Galeckas, M. Salumaa, F. Ducroquet, and E. Rauwel, "Photocurrent generation in carbon nanotube/cubic-phase HfO2 nanoparticle hybrid nanocomposites," *Beilstein J. Nanotechnol.*, vol. 7, pp. 1075–1085, 2016.

[2] M. Salumaa, "Hybrid nanomaterials based on carbon nanotubes and metal oxide nanoparticles for photovoltaic applications," 2015.

[3] A. Aasna, "Hybrid nanomaterials based on carbon nanotubes and metal oxide nanoparticles for energy harvesting applications," 2016.

[4] D. Ludington, "Tips for Measuring Small Currents," *Circuit Cellar*, 2014. [Online]. Available: https://circuitcellar.com/cc-blog/tips-for-measuring-small-currents/. [Accessed: 30-Mar-2020].

[5] D. L. Jones, "The uCurrent Specification Sheet," pp. 1–19, 2010.

[6] "CoE EQUiTANT." [Online]. Available: https://kbfi.ee/chemical-physics/centre-of-excellence-134/?lang=en. [Accessed: 10-May-2020].

[7] M. Nanko, "Definitions and Categories of Hybrid Materials," *AZojomo*, vol. 6, 2009.

[8] ISO/TC 229, "ISO/TS 80004-2:2015. Nanotechnologies -- Vocabulary -- Part 2: Nano-objects," vol. 2015. 2015.

[9] S. Ramanathan, S. C. B. Gopinath, M. K. Md. Arshad, and P. Poopalan, "Multidimensional (0D-3D) nanostructures for lung cancer biomarker analysis: Comprehensive assessment on current diagnostics," *Biosens. Bioelectron.*, vol. 141, 2019.

[10] S. Contera, "Interfaces and Mechanical Properties of Nanomaterials and Biological Systems with AFM," 2012. [Online]. Available: https://www.azonano.com/article.aspx?ArticleID=3012. [Accessed: 21-May-2020].

[11] J. S. Silfies, S. A. Schwartz, and M. W. Davidson, "The Diffraction Barrier in Optical Microscopy." [Online]. Available: https://www.microscopyu.com/techniques/super-resolution/the-diffraction-barrier-in-optical-microscopy. [Accessed: 21-May-2020].

[12] R. R. Wagner and R. M. Krug, "Virus," *Encyclopaedia Britannica*, 2020. [Online]. Available: https://www.britannica.com/science/virus/Size-and-shape. [Accessed: 21-May-2020].

[13] B. Cuffari, "What Nanomaterials Exist in Nature?," 2018. [Online]. Available:

https://www.azonano.com/article.aspx?ArticleID=4837.

[14] A. Mayer, J. Czerwinski, M. Kasper, A. Ulrich, and J. J. Mooney, "Metal oxide particle emissions from diesel and petrol engines," *SAE Technical Papers*, 2012. [Online]. Available: https://www.sae.org/publications/technical-papers/content/2012-01-0841/.

[15] "Diesel Exhaust Particle Size," 2016. [Online]. Available: https://dieselnet.com/tech/dpm_size.php. [Accessed: 21-May-2020].

[16] P. Rauwel, E. Rauwel, C. Persson, M. F. Sunding, and A. Galeckas, "One step synthesis of pure cubic and monoclinic HfO2 nanoparticles: Correlating the structure to the electronic properties of the two polymorphs," *J. Appl. Phys.*, vol. 112, no. 10, 2012.

[17] S. P. Goutam, G. Saxena, D. Roy, A. K. Yadav, and R. N. Bharagava, "Green Synthesis of Nanoparticles and Their Applications in Water and Wastewater Treatment," *Bioremediation Ind. Waste Environ. Saf.*, pp. 349–379, 2020.

[18] R. N. Wijesena, "Top-down methods," *Ninithi*. [Online]. Available: https://ninithi.wordpress.com/topdown_methods/. [Accessed: 22-May-2020].

[19] "Nanoparticle production – How nanoparticles are made." [Online]. Available: https://www.nanowerk.com/how_nanoparticles_are_made.php.

[20] "Physical methods," *Nanoshel*. [Online]. Available: https://www.nanoshel.com/physical-methods/. [Accessed: 22-May-2020].

[21] S. P. Sajjadi, "Sol-gel process and its application in Nanotechnology," *J. Polym. Eng. Technol.*, vol. 13, pp. 38–41.

[22] Aerogel.org, "The Sol-Gel Process." [Online]. Available: http://www.aerogel.org/?p=992.

[23] M. Niederberger, "Nonaqueous sol-gel routes to metal oxide nanoparticles," *Acc. Chem. Res.*, vol. 40, no. 9, pp. 793–800, 2007.

[24] I. Bilecka and M. Niederberger, "New developments in the nonaqueous and/or non-hydrolytic sol-gel synthesis of inorganic nanoparticles," *Electrochim. Acta*, vol. 55, no. 26, pp. 7717–7725, 2010.

[25] S. Iravani, H. Korbekandi, S. V. Mirmohammadi, and B. Zolfaghari, "Synthesis of silver nanoparticles: Chemical, physical and biological methods," *Res. Pharm. Sci.*, vol. 9, no. 6, pp. 385–406, 2014.

[26] H. Nadaroglu, A. Alayli, and S. Ince, "Synthesis of Nanoparticles by Green Synthesis Method," *Internatio nal J. Innov. Res. Rev.*, vol. 1, no. 1, pp. 6–9, 2017.

[27] M. Monthioux and V. L. Kuznetsov, “Who should be given the credit for the discovery of carbon nanotubes?,” *Carbon N. Y.*, vol. 44, no. 9, pp. 1621–1623, Aug. 2006.

[28] M. Terrones, “Science and Technology of the Twenty-First Century: Synthesis, Properties, and Applications of Carbon Nanotubes,” *Annu. Rev. Mater. Res.*, vol. 33, no. 1, pp. 419–501, 2003.

[29] E. Gregersen, “Van der Waals forces.” [Online]. Available: https://www.britannica.com/science/van-der-Waals-forces. [Accessed: 12-May-2020].

[30] J. Than, “Van Der Waals Interactions,” 2019. [Online]. Available: https://chem.libretexts.org/Bookshelves/Physical_and_Theoretical_Chemistry_Textbook_Maps/Supplemental_Modules_(Physical_and_Theoretical_Chemistry)/Physical_Properties_of_Matter/Atomic_and_Molecular_Properties/Intermolecular_Forces/Specific_Interactions/Va. [Accessed: 12-May-2020].

[31] T. Pedersen, “Facts About Hafnium,” 2018. [Online]. Available: https://www.livescience.com/38591-hafnium.html. [Accessed: 22-May-2020].

[32] A. Augustyn, “Hafnium,” *Encyclopaedia Britannica*. [Online]. Available: https://www.britannica.com/science/hafnium. [Accessed: 22-May-2020].

[33] “Hafnium dioxide: Toxicological Summary,” *ECHA*. [Online]. Available: https://echa.europa.eu/registration-dossier/-/registered-dossier/12508/7/1. [Accessed: 25-May-2020].

[34] Intel, “Intel’s Fundamental Advance in Transistor Design Extends Moore’s Law, Computing Performance,” 2007. [Online]. Available: https://www.intel.com/pressroom/archive/releases/2007/20071111comp.htm. [Accessed: 22-May-2020].

[35] E. Rauwel, A. Galeckas, and P. Rauwel, “Photoluminescent cubic and monoclinic HfO2 nanoparticles: Effects of temperature and ambient,” *Mater. Res. Express*, vol. 1, no. 1, 2014.

[36] P. Rauwel, A. Galeckas, F. Ducroquet, and E. Rauwel, “Selective photocurrent generation in HfO 2 and carbon nanotube hybrid nanocomposites under Ultra-Violet and visible photoexcitations,” *Mater. Lett.*, vol. 246, pp. 45–48, 2019.

[37] “ITO Coatings,” *Präzisions Glas & Optik GmbH*. [Online]. Available: https://www.pgo-online.com/intl/ito.html. [Accessed: 22-May-2020].

[38] Akolk1, “DIY Solar Cell From Scratch,” *instructables.com*. [Online]. Available:

https://www.instructables.com/id/DIY-solar-cell-from-scratch/. [Accessed: 22-May-2020].

[39] J. Gotro, "Dielectric Cure Monitoring Part 12: Dielectric Sensors," *Polymer Innovation Blog*, 2015. [Online]. Available: https://polymerinnovationblog.com/dielectric-cure-monitoring-part-12-dielectric-sensors/. [Accessed: 22-May-2020].

[40] R. D. A. A. Rajapaksha, N. A. N. Yahaya, M. N. A. Uda, and U. Hashim, "Development of portable electronic reader for picoampere detection for two-electrode based amperometric biosensor applications," *AIP Conf. Proc.*, vol. 2045, no. December, pp. 1–7, 2018.

[41] "Making OLEDs and OPVs: A Quickstart Guide." [Online]. Available: https://www.ossila.com/pages/guide-to-making-organic-photovoltaics-solar-cells-or-organic-light-emitting-diodes-oleds. [Accessed: 22-May-2020].

[42] Agilent Technologies, "Agilent 4155C Semiconductor Parameter Analyzer Agilent 4156C Precision Semiconductor Parameter Analyzer," 2003. [Online]. Available: https://testequipmentconnection.com/specs/AGILENT-HP_4156C-410.PDF. [Accessed: 09-May-2020].

[43] B. D. Viezbicke, S. Patel, B. E. Davis, and D. P. Birnie, "Evaluation of the Tauc method for optical absorption edge determination: ZnO thin films as a model system," *Phys. status solidi*, vol. 252, no. 8, pp. 1700–1710, Aug. 2015.

[44] R. Nave, "DeBroglie Wavelength," *HyperPhysics*, 2016. [Online]. Available: http://hyperphysics.phy-astr.gsu.edu/hbase/quantum/debrog2.html. [Accessed: 25-May-2020].

[45] "Keysight (Agilent) 4155A Data Sheet." .

[46] Agilent Technologies, "HP4155A Semiconductor Parameter Analyzer User's Task Guide." [Online]. Available: https://www.keysight.com/upload/cmc_upload/All/04155-90015.pdf.

[47] D. Johnson-Davies, "Nano Current Meter," *technoblogy.com*, 2019. [Online]. Available: http://www.technoblogy.com/show?2S67. [Accessed: 22-May-2020].

[48] "Solar Cell I-V Test System," *Ossila*. [Online]. Available: https://www.ossila.com/products/solar-cell-iv-test-system?variant=13633049100384. [Accessed: 22-May-2020].

[49] Keithley Instruments inc., *Low Level Measurements Handbook*. 2013.

[50] "HP-39C Digital Multimeter," *HoldPeak*. [Online]. Available: https://holdpeak-

store.com/hp-39c-digital-multimeter-auto-range-tester-ac-ac-6000-counts-true-rms-ncv-ohm-frequency-diode-transistor-tester-esr/. [Accessed: 31-Mar-2020].

[51] H. Asmussen, *HM8112-3 6½-Digit Precision Multimeter Benutzerhandbuch*. HHAMEG Instruments GmbH, 2015.

[52] "L78 datasheet," *STMicroelectronics*, 2018. [Online]. Available: https://www.st.com/resource/en/datasheet/l78.pdf.

[53] "L79 datasheet," *STMicroelectronics*, 2018. [Online]. Available: https://www.st.com/resource/en/datasheet/l79.pdf. [Accessed: 24-May-2020].

[54] "TL081 datasheet," *STMicroelectronics*, 2008. .

[55] "ICL7660S, ICL7660A Datasheet," *Renesas*, 2020. [Online]. Available: https://www.renesas.com/eu/en/www/doc/datasheet/icl7660s-a.pdf. [Accessed: 24-May-2020].

[56] R. Baddi, "Nano-Ampere Meter," *Electronicsforu.com*, 2011. [Online]. Available: https://www.electronicsforu.com/electronics-projects/nano-ampere-meter. [Accessed: 30-Mar-2020].

[57] I. Poole, "Op Amp Gain: explanation & equations," *Electronics Notes*. [Online]. Available: https://www.electronics-notes.com/articles/analogue_circuits/operational-amplifier-op-amp/gain-equations.php. [Accessed: 25-May-2020].

[58] Gigahertz-Optik GmbH, "MSC15." [Online]. Available: https://www.gigahertz-optik.de/en-us/product/msc15/getpdf. [Accessed: 25-May-2020].

[59] Welljoin, "Performance specifications of ITO conductive film layer." [Online]. Available: https://www.amazon.com/Welljoin-Conductive-50x40x1-1mm-Transparent-Indium/dp/B07FYDL8XH. [Accessed: 27-May-2020].

[60] "Carbon film resistor," *resistorguide.com*, 2019. [Online]. Available: http://www.resistorguide.com/carbon-film-resistor/. [Accessed: 26-May-2020].

[61] "Precison metal film fixed resistors," *Royalohm.com*, 2007. [Online]. Available: http://data.oomipood.ee/pdf//M0_6.pdf.

ÜLDKOKKUVÕTE

PROTOTÜÜPSEADE FOTOGALVAANILISE EFEKTIGA VOOLU TEKITAMISEKS KASUTADES AKTIIVSE KIHINA HfO_2-SÜSINIK-NANOTORUDE HÜBRIIDE

Nanohübriidid on ained, kus materjalid on ühendatud nanomeetrites mõõdetava suurusega osakestena või molekulaarsel tasemel loodud keemiliste sidemete abil. Ainet nimetatakse nanotehnoloogiliseks, kui osakese vähemalt üks dimensioon on väiksem kui 100 nm. Tavalistes komposiitmaterjalides mis on saadud jahvatamise, purustamise, segamise ja sulatamise viisil, on esindatud kõigi lisatud ainete omadused ja sellist segamist kasutatakse ühe aine omaduste parandamiseks teise aine lisamise teel. Nanomaterjalides võivad aga hübridiseerumisel avalduda uued omadused, mis puhastel ainetel puuduvad. Ühes eelnevas uuringus tuvastati hafniumdioksiidi (HfO_2) ja CNT nanohübriidide võime tekitada fotovoolu UV või nähtava valgusega kiiritamise tulemusena. Sellest tuleneb põhjendatud vajadus neid nanohübriide edasi uurida, et välja selgitada nende potentsiaal energiatootmisel või sensoritena kasutamise eesmärkidel.

Selle töö eesmärk oli leida parim viis piiratud ressursside puhul nanohübriidmaterjalide valgusega kiiritamiseks ja selle tulemusel tekkinud fotovoolu mõõtmiseks. Lahendamist vajav probleem antud juhul oli see, et eeldatavasti on tekkiv vool nanoamprite suurusjärgus ja taskukohaste multimeetrite mõõtevahemik algab mikroamprite piirkonnas. Samuti segavad nanoamprite suurusjärgus tehtavaid mõõtmisi erinevad indutseerivad häireallikad, näiteks lähedal asuvad vooluallikad ja mõõdetavast voolust oluliselt tugevama vooluga juhtmed. Siiani on nanohübriidmaterjalide elektriliste omaduste mõõtmiseks kasutatud Prantsusmaal, University Grenoble Alpes ülikooli uurimiskeskuse MINATEC IMEP-LaHC laboratooriumi seadmeid. Piisava täpsusega mõõtmisviisi leidmisel saaks edasisi arendustegevuse käigus vajalikke mõõtmisi teha kohapeal.

Nanosuuruses voolude mõõtmiseks ei ole soodsaid mõõtevahendite valmislahendusi olemas ja kirjanduse uurimise järgi peavad need, kel seda vaja teha on, ostma endale kalli täppismultimeetri või koostama endale mõne operatsioonivõimendi baasil eelvõimendi. See meetod võeti kasutusele ka selles töös.

Valgustuseks kasutati valgusdioode (LED) mis emiteerivad UV ja valge liitvalguse piirkonnas. UV LEDid osteti lainepikkusega 365 nm, kuid kontrollimise tulemusena saadi nende kiiratavaks peamiseks lainepikkuseks 372 nm. UV valgust kasutati seetõttu, et eelnevate uuringute tulemusena on tehtud kindlaks, et vastav nanohübriidmaterjal omandab madalama lainepikkusega kiirgust paremini. Valgustamiseks kasutati üheksat 1 W võimsusega LEDi ja kolme sama võimsusega valge valguse LEDi, mis olid proovile suunatud 50 mm kauguselt. Üllatavaks probleemiks osutus nendele LEDidle hoidja ja reflektori leidmine ja konstrueerimine. Mõõdetud UV valguse erivõimsus 9 LEDi puhul oli 339 W/m^2 kohta.

Uurimistöös kasutati proovimaterjalina HfO_2-CNT nanohübriidmaterjali. Proovide hoidmiseks ja proovist saadava fotovoolu koormusele juhtimiseks valmistati trükkplaadist söövitatud vasest kammelektroodiga alused (3 tk), suurusega 15 × 18 mm. Alusele tilgutati nanohübriidmaterjaliga etanoolilahus ja lasti etanoolil aurustuda. Mõõtmistulemus mõõdeti aluse klemmidelt. Lisaks kammelekroodile kasutati voolu juhtiva läbipaistva indium-tina oksiidi (ITO) kihiga kaetud klaasi tükke, kaks klaasi vastakuti ja nanomaterjali proov nende vahel. Kokkuvõttes osutusid kammelektroodid oluliselt mugavamalt kasutatavateks. Mõõtmistel problemaatiliseks osutus klaas-elektroodi kinnitamine alusele sellisel viisil, et sama kinnitust saaks kasutada nii kamm- kui klaaselektroodi puhul. Proove kiiritati UV valgusega lainepikkusel 372 nm ja proovi kontaktidelt mõõdeti mõõtetulemus enne valgusseadmega kiiritamist ja kiiritamise ajal. Mõõtmisel kasutati kahte multimeetrit, 1) täppismultimeetrit Hameg HM8112-3, mille eraldusvõime on 1 nA või 0,1 nA sõltuvalt integratsiooniajast ja 2) kantavat multimeetrit HoldPeak HP-39C, mille eraldusvõime alalisvoolu mõõtmisel on 0,1 µA (100 nA). Viimase puhul tuli kasutusele võtta töö peamise osana koostatud eelvõimendi, mis võimaldas tavalise multimeetriga mõõta voolu alates 0,01 nA.

Töös kasutatud eelvõimendi peamiseks osaks on operatsioonivõimendi TL081. See võimendab mõõteahelas oleval šunttakistil tekkivat pingelangu ja selle väljundiks on millivoltide mõõtevahemikus pinge. Võimenduse suurus on määratud kahe takisti suhtega, antud skeemis on see 100. Operatsioonivõimendi teises sisendis on mõõtevahemikku määravad takistid suurusega 1, 10 ja 100 kΩ. Operatsioonivõimendil on bipolaarne toitepinge: +5 V ja -5 V ning skeemi toidetakse 9 V patareiga. Pinge langetamiseks on

koostatud skeem, mis koosneb L78 ja L79 +5 V ja -5 V pingeregulaatoritest ja ICL7660 pingeinverterist. Eelvõimendi skeem on töös joonisel 11.

Töös arvutati välja eelvõimendi ja multimeetrite mõõtemääramatus, milleks oli eelvõimendi puhul (± 1 nA), Hamegi multimeetri puhul mikroamprite mõõtevahemikus (± 0,0044 nA) ja HoldPeaki puhul millivoltide mõõtevahemikus (± 0,3 mV). Tavalist multimeetrit koos eelvõimendiga kasutades tuleb arvestada mõlema määramatusega. Eelvõimendi määramatus on võrdlemisi suur, sest selle määramatuse määravad selles kasutatud takistite täpsusklassid ja antud juhul kasutati 5 % täpsusklassi takisteid. 1 % täpsusklassi takisteid kasutades saaks määramatuseks ± 0,2 nA.

Mõõteskeemi kalibreerimine ja katsetamine oli kavas teha Prantsusmaal, Grenobles asuvas laboris koos sealsete täppismõõteseadmete ja kohapealsete nanomaterjalide mõõtmisega, kuid koroonaviiruse leviku tõttu lükkus see tulevikku. Selle asemel kontrolliti esialgset mõõtevõimekust HoldPeaki multimeetriga. Selleks koostati vooluahel 2,57 V toiteallikast ja erinevatest takistitest vahemikus 1 MΩ kuni 20 MΩ. Koormusel tekkinud voolu mõõdeti multimeetriga otse ja läbi eelvõimendi. Saadud mõõtetulemust võrreldi Oomi seaduse alusel arvutatud väärtusega. Töös olevas tabelis 5 on vastavad arvud ära toodud. Selle tulemusel saab järeldada, et mõõteskeem töötab, ja täpsus piisab selleks, et tuvastada lootustandvaid nanohübriimaterjale, kuid edasiseks kasutamiseks oleks siiski vaja kasutusele võtta parema täpsusklassi takistid ja kalibreerida skeem mõne täppismultimeetriga.

Prototüüpide arendamise käigus tehti mõõtmised kammelektroodi ja nanohüübriid-materjalide proovidega. Saadud tulemused on tabelis 6. ja joonisel 24. Esimesel kahel mõõtmistel kasutati multimeetrit Hameg ja mõõdeti otse mikroamprite piirkonnas. Esimese prototüübiga saadi proovi poolt genereeritud fotovoolu tugevuseks 20 nA, kuid müratau st oli 50 nA ja mõõtetulemus oli väga kõikuv erinevate häirete tõttu. Teisel mõõtmisel oli järgmise prototüübi puhul lisatud valgusdioodide toiteplokkide varjestus ja see vähendas mõnevõrra müratausta, 41 nA peale, kuid ka proovidest saadav vool oli väiksem, 7 nA. Selle mõõtmise puhul aga multimeetri näit enam ei kõikunud. Viimase valmis saanud prototüübi puhul tehti mõõtmised eelvõimendit ja HoldPeaki multimeetrit kasutades. Samuti oli prototüübis kasutusel oluliselt rohkem häireid varjestavaid meetodeid ja müratau st oli ainult 1,7 nA ja näit oli stabiilne. Samuti vähenes jätkuvalt proovist saadav fotovool, kuid seekord

oli see fotovool suurem kui müratаust, ühe aluse puhul 2,3 nA. Oluline antud töö kontekstis on see, et häired on vähendatud oluliselt väiksemaks kui eeldatavalt mõõdetav vool ja tõestatud on seadme nanovoolu mõõtmise võime, eraldusvõimega kuni 0,01 nA.

Töö eesmärk oli koostada mõõteseade, millega saab kiiritada nanohübriidmaterjali proovi ja mõõta sellest resulteeruvat fotovoolu. Selle saavutamiseks uuriti kirjandusest, kuidas on varem tegeldud nanosuuruses voolude mõõtmisega ja koostati neli prototüüpseadet, millest iga järgmine kõrvaldas eelmise testimisel välja tulnud probleemid. Viimasel valminud prototüübil oli operatsioonivõimendi baasil eelvõimendi, millega sai mõõta nanovoolu eraldusvõimega kuni 0,01 nA, vajamata selleks kallist mõõteriista. Esimestel prototüüpidel probleemiks osutunud häirete tase saadi hästi kontrolli alla, viimasel oli see 1,7 nA. Ka viimasel prototüübil kaardistati parendusvõimalused ja esitati need nimekirjana töö peamises osas. Peamiselt vajab tuleviku töös edasiarendust kasutusmugavus ja portatiivsus. Olemasolevat prototüüpi edasi arendades saab koostada seadme, mis suudab tekitada piisava fotovoolu ja seda mõõtes aitab teadlastel selekteerida lootustandvaid nanohübriidmaterjale Tartus kohapeal.

APPENDIXES

LIHTLITSENTS

Lisa 1. Lihtlitsents lõputöö salvestamiseks ja üldsusele kättesaadavaks tegemiseks ning juhendajate kinnitus lõputöö kaitsmisele lubamise kohta

Mina, Toivo Viidalepp,
sünniaeg 18.02.1982,

1. annan Eesti Maaülikoolile tasuta loa (lihtlitsentsi) enda koostatud lõputöö

Fabrication of a Prototype Device for Photocurrent Generation Using HfO_2-CNT Nanohybrids as the Active Layer,

mille juhendaja(d) on Protima Rauwel, Alo Allik ja Erwan Rauwel,

1.1. salvestamiseks säilitamise eesmärgil,
1.2. digiarhiivi DSpace lisamiseks ja
1.3. veebikeskkonnas üldsusele kättesaadavaks tegemiseks

kuni autoriõiguse kehtivuse tähtaja lõppemiseni;

2. olen teadlik, et punktis 1 nimetatud õigused jäävad alles ka autorile;
3. kinnitan, et lihtlitsentsi andmisega ei rikuta teiste isikute intellektuaalomandi ega isikuandmete kaitse seadusest tulenevaid õigusi.

Lõputöö autor Toivo Viidalepp
/ allkirjastatud digitaalselt /

Tartu, / kuupäev on digiümbrikus /

Juhendaja(te) kinnitus lõputöö kaitsmisele lubamise kohta

Luban lõputöö kaitsmisele.

Protima Rauwel / kuupäev on digiümbrikus /
/ allkirjastatud digitaalselt /

Alo Allik / kuupäev on digiümbrikus /
/ allkirjastatud digitaalselt /

Erwan Rauwel / kuupäev on digiümbrikus /
/ allkirjastatud digitaalselt /